Role of Riverine Dissolved Organic and Inorganic Carbon and Nutrients in Global-ocean Air-sea CO_2 Fluxes

Raphaël Savelli[1], Dustin Carroll[2,1], Dimitris Menemenlis[1], Stephanie Dutkiewicz[3,4], Manfredi Manizza[5], Anthony Bloom[1], Karel Castro-Morales[6], Charles E. Miller[1], Marc Simard[1], Kevin W. Bowman[1], Hong Zhang[1]

[1]Jet Propulsion Laboratory, California Institute of Technology, Pasadena, CA, USA
[2]Moss Landing Marine Laboratories, San José State University, Moss Landing, CA, USA
[3]Department of Earth, Atmospheric and Planetary Sciences, Massachusetts Institute of Technology, Cambridge, Massachusetts, USA
[4]Center for Global Change Science, Massachusetts Institute of Technology, Cambridge, Massachusetts, USA
[5]Geosciences Research Division, Scripps Institution of Oceanography, University of California San Diego, La Jolla, California, USA
[6]Institute of Biodiversity, Aquatic Geomicrobiology, Friedrich Schiller University, Jena, Germany

Key Points:

- We assess how global lateral exports impact air-sea CO_2 flux and carbon cycling in ECCO-Darwin ocean biogeochemistry simulations
- Near river mouths, changes in CO_2 flux are dominated by the solubility pump and lead to outgassing
- Further offshore, riverine nitrogen leads to increased CO_2 uptake via phytoplankton fertilization

Corresponding author: Dustin Carroll, `dustin.carroll@sjsu.edu`

Abstract

While the preindustrial ocean was assumed to be in equilibrium with the atmosphere, the modern ocean is a carbon sink, resulting from natural variability and anthropogenic perturbations, such as fossil fuel emissions and changes in riverine exports over the past two centuries. Here we use a suite of sensitivity experiments based on the ECCO-Darwin global-ocean biogeochemistry model to evaluate the response of air-sea CO_2 flux and carbon cycling to present-day lateral fluxes of carbon, nitrogen, and silica. We generate a daily export product by combining point-source freshwater discharge from JRA55-do with the Global NEWS 2 watershed model, accounting for lateral fluxes from 5171 watersheds worldwide. From 2000 to 2019, carbon exports increase CO_2 outgassing by 0.22 Pg C yr^{-1} via the solubility pump, while nitrogen exports increase the ocean sink by 0.17 Pg C yr^{-1} due to phytoplankton fertilization. On regional scales, exports to the Tropical Atlantic and Arctic Ocean are dominated by organic carbon, which originates from terrestrial vegetation and peats and increases CO_2 outgassing (+10 and +20%, respectively). In contrast, Southeast Asia is dominated by nitrogen from anthropogenic sources, such as agriculture and pollution, leading to increased CO_2 uptake (+7%). Our results demonstrate that the magnitude and composition of riverine exports, which are determined in part from upstream watersheds and anthropogenic perturbations, substantially impact present-day regional-to-global-ocean carbon cycling. Ultimately, this work stresses that lateral fluxes must be included in ocean biogeochemistry and Earth System Models to better constrain the transport of carbon, nutrients, and metals across the land-ocean-aquatic-continuum.

Plain Language Summary

Due to ongoing climate change and human activities, the transport of carbon and nutrients from rivers to the ocean has changed, with rivers now contributing to the modern ocean's sequestration of atmospheric carbon dioxide (CO_2). In this study, we add the effect of present-day rivers to a numerical model of the ocean carbon cycle (ECCO-Darwin) and then estimate their impact on air-sea CO_2 exchange and ocean biogeochemistry. Over a 20-year period, riverine carbon saturates the surface ocean and increases the amount of CO_2 released to the atmosphere, while nitrogen fertilizes phytoplankton and increases the capture of atmospheric CO_2 via photosynthesis. In the Tropical Atlantic and Arctic Oceans, organic carbon drained from vegetation and peats causes outgassing of ocean carbon. In Southeast Asia, the large amount of riverine nitrogen originating from human activities, such as agriculture or waste water, increases ocean CO_2 sequestration. Our work highlights how rivers, which are affected by present-day human actions and climate change, impacts the ocean's carbon cycle across regional-to-global scales.

1 Introduction

Globally, shelf and marginal seas are typically sinks of CO_2, where uptake driven by strong biological productivity exceeds outgassing from organic matter degradation and carbon enrichment by river runoff and coastal upwelling (Ianson et al., 2009; W.-J. Cai, 2011; W. Cai et al., 2013; Laruelle et al., 2017; Bertin et al., 2023). Rivers transport roughly 0.8–0.9 Pg C yr^{-1} from land to coastal regions as dissolved organic carbon (DOC), dissolved inorganic carbon (DIC), particulate organic carbon (POC), and particulate inorganic carbon (PIC); a third of the aforementioned total riverine export of carbon is buried in coastal sediments (Regnier et al., 2022; Battin et al., 2023). Nutrients such as phosphorus, nitrogen, and silica are also conveyed by rivers along with carbon. Terrestrial inorganic carbon and nutrients in streams originate from weathering of the lithosphere and the associated sink of atmospheric CO_2, along with the remineralization of organic matter in streams and/or on land (Suchet & Probst, 1995; Battin et

al., 2023). Riverine organic carbon and nutrients are further supplemented by primary production from land vegetation and organic matter mobilized through direct literfall, runoff, leaching, and erosion into rivers (Meybeck & Vörösmarty, 1999; Seitzinger et al., 2010; Regnier et al., 2013; Battin et al., 2023).

Once injected into the coastal ocean, riverine carbon is generally outgassed back to the atmosphere in the form of CO_2, due to the saturation of surface-ocean waters by terrestrial DIC and remineralization of terrestrial organic matter (Hartmann et al., 2009; Lacroix et al., 2020; Bertin et al., 2023) in shallow, well-mixed water columns. The natural transport of carbon from terrestrial ecosystems to ocean outgassing, the so-called "river loop", is estimated to be 0.65 ± 0.3 Pg C yr^{-1} (Regnier et al., 2022; Friedlingstein et al., 2023). With respect to inorganic nutrients, their injection into the surface ocean can fertilize growth of photosynthetic organisms in nutrient-limited regions. Globally, this lateral flux increases ocean primary productivity and contributes to a coastal-ocean sink of $\sim$0.25 Pg C yr^{-1}, which is roughly 17% of the global-ocean sink (W.-J. Cai, 2011; Lacroix et al., 2021; S. Gao et al., 2023).

Over the past two centuries, terrestrial anthropogenic perturbations have led to a substantial increase in the load of nitrogen and phosphorus through agricultural fertilization, leaked sewage, and land-use change (Smith et al., 2003; Lee et al., 2016; Lacroix et al., 2021). Projections of the historical riverine dissolved nitrogen and phosphorus load depict a three- to four-fold increase over the period 1900–2019 (Lacroix et al., 2021). When delivered in excessive amounts, these nutrients can alter aquatic and ocean ecosystems, resulting in eutrophication, hypoxia, and acidification in coastal waters (Laurent et al., 2017; Fennel & Testa, 2019). Dissolved and particulate carbon are also affected regionally by agricultural liming, the addition of sulfuric acid to watersheds, changes in erosion patterns, and river management (Monteith et al., 2007; Raymond et al., 2008; Calmels et al., 2007; Regnier et al., 2013; Maavara et al., 2017). Projected trends for river biogeochemical loads remain uncertain and exhibit disparate regional responses over the 21^{st} century depending on the chosen shared socioeconomic pathway (Beusen et al., 2022; Beusen & Bouwman, 2022; Vishwakarma et al., 2022; Zhang et al., 2022).

While present estimates of riverine freshwater and biogeochemical fluxes are poorly sampled in space and time, land surface and watershed models can provide spatiotemporally-resolved lateral exports at global scales (Mayorga et al., 2010; Krinner et al., 2005; Hagemann & Dümenil, 1997; Hagemann & Gates, 2003; M. Li et al., 2017; Bloom et al., 2020). Coupled with ocean biogeochemical models, it is thus possible to quantify the response of the coastal and open-ocean carbon cycle to lateral fluxes (Lacroix et al., 2020, 2021; Mathis et al., 2022; Louchard et al., 2021; da Cunha & Buitenhuis, 2013; Le Fouest et al., 2013; S. Gao et al., 2023; Bertin et al., 2023). Regarding the importance of lateral exports in ocean carbon cycling, it is critical that ocean biogeochemical models better account for coastal mechanisms occurring across the land-ocean-aquatic-continuum (LOAC) (Ward et al., 2020; Mathis et al., 2022). Such improvements will come from 1) finer horizontal and vertical grid resolution to resolve small-scale ocean physics (vertical mixing, submesoscale processes) and associated biology (hypoxia, phytoplankton blooms) and 2) improved representation of LOAC components (river and groundwater discharge, bottom sediment diagenesis, and estuarine biogeochemical filtering) (Ward et al., 2020; Sharples et al., 2017). While recent modeling efforts have made improvements in this regard (Volta et al., 2016; Laruelle et al., 2017; Mathis et al., 2022, 2024), the respective contribution of riverine exports to air-sea CO_2 fluxes across the global ocean remains to be assessed.

In this study, we add lateral fluxes of carbon and nutrients to the ECCO-Darwin global-ocean biogeochemistry state estimate (Carroll et al., 2020, 2022) and evaluate the response of air-sea CO_2 flux and ocean biogeochemistry to daily point-source river forcing from 2000–2019. We compute daily riverine biogeochemical export by combining point-source freshwater discharge from the JRA55-do atmospheric reanalysis with the Global NEWS 2 watershed model (Mayorga et al., 2010; Suzuki et al., 2018; Tsujino et al., 2018;

Feng et al., 2021). We then investigate the respective contribution of dissolved organic and inorganic carbon, nitrogen, and silica to air-sea CO_2 fluxes at coastal, basin, and global scales, as performed in Lacroix et al. (2020). This paper provides new tools and methods for improved estimates of how riverine biogeochemical exports impact ocean carbon cycling, which is pivotal for understanding the response of ocean biogeochemistry to anthropogenic perturbations on land.

2 Methods

2.1 The ECCO-Darwin Ocean Biogeochemistry State Estimate

The ECCO-Darwin ocean biogeochemistry state estimate is extensively described in Brix et al. (2015), Manizza et al. (2019) and Carroll et al. (2020, 2022, 2024). For the ECCO-Darwin solution presented in this paper, ocean physics (circulation, temperature, salinity, and sea ice) are provided by the Estimating the Circulation and Climate of the Ocean (ECCO) global-ocean and sea-ice data synthesis version 4 release 5 (V4r5) (Forget et al., 2015).

The horizontal grid is based on the LLC90 (Lat-Lon-Cap 90) grid, which is described in detail in (Forget et al., 2015). The nominal horizontal grid resolution in ECCO v4 LLC90 is 1°(∼55 km at high latitudes). The vertical discretization consists of 50 z-levels, ranging from 10-m thickness in the top 7 levels to 450 m at depth. ECCO v4 uses a third-order, direct-space-time tracer advection scheme in the horizontal and an implicit third-order upwind scheme in the vertical; a time step of 3600 s is used. Vertical mixing is parameterized using the Gaspar–Grégoris–Lefevre (GGL) mixing-layer turbulence closure and convective adjustment scheme (Gaspar et al., 1990). ECCO v4 assimilates physical observations via the 4-D adjoint method (Wunsch et al., 2009; Wunsch & Heimbach, 2013).

Daily river runoff in the present configuration is based on the Japanese 55-year atmospheric reanalysis (JRA55-do) river forcing dataset, which uses the CaMa-Flood global river routing model and adjusted runoff from the land component of JRA-55 (Suzuki et al., 2018; Tsujino et al., 2018; Feng et al., 2021). Point source JRA55-do freshwater runoff (m s^{-1}) was added to ECCO v4 as a real freshwater flux in the surface ocean (first vertical level) at the closest ECCO v4 LLC90 grid cell along the coastal periphery. The freshwater flux was adjusted according to the difference in grid cell area between JRA55-do (0.25°x 0.25°) and ECCO v4 LLC90. A full evaluation of ocean physics from ECCO v4 LLC90 compared to observations can be found in the Supporting Information and Feng et al. (2021).

ECCO v4 LLC90 ocean physics was coupled online with the Massachusetts Institute of Technology Darwin Project ecosystem model described in Brix et al. (2015). The ecosystem model solves 39 prognostic variables such as carbon, nitrogen, phosphorus, iron, silica, oxygen, and alkalinity. The model simulates their respective cycle from inorganic pools to living/dead matter of plankton organisms and the subsequent remineralization, all driven by the ocean physics. The carbonate chemistry is solved by the method in Follows et al. (2006). Plankton species consist of five large-to-small functional phytoplankton types (diatoms, other large eukaryotes, *Synechococcus*, and low- and high-light adapted *Prochlorococcus*), and two zooplankton types. Atmospheric CO_2 partial pressure at sea level ($apCO_2$) from the National Oceanic and Atmospheric Administration Marine Boundary Layer Reference product (Andrews et al., 2014) was used to drive air-sea CO_2 fluxes computed by the model according to Wanninkhof (1992). Atmospheric iron dust is deposited at the ocean surface based on the monthly climatology of Mahowald et al. (2009). Once at the ocean bottom, particulate inorganic and organic matter is removed at the sinking rate to limit the accumulation of particulates on the seafloor. Biogeochemical observations were used to optimize the biogeochemical model using a Green's

Functions approach (Menemenlis et al., 2005); the optimization methodology and associated data are fully described in Carroll et al. (2020). The ECCO-Darwin solution was previously published using monthly climatological freshwater runoff forcing from Fekete et al. (2002). Here, the Baseline simulation consists of the same ocean biogeochemistry simulation as Carroll et al. (2020), but with daily point-source freshwater runoff from January 1992 to December 2019. To allow partial adjustment to these new boundary conditions, the analysis period hereinbelow spans the last 20 years of the simulation, January 2000 to December 2019. Figure 1 shows the general match-up between time-mean ECCO-Darwin air-sea CO_2 fluxes and the MPI SOM FFN v2022 (Landschützer et al., 2016; Jersild et al., 2023) and Jena CarboScope v2023 (Rödenbeck et al., 2013) products for the 2000–2019 study period.

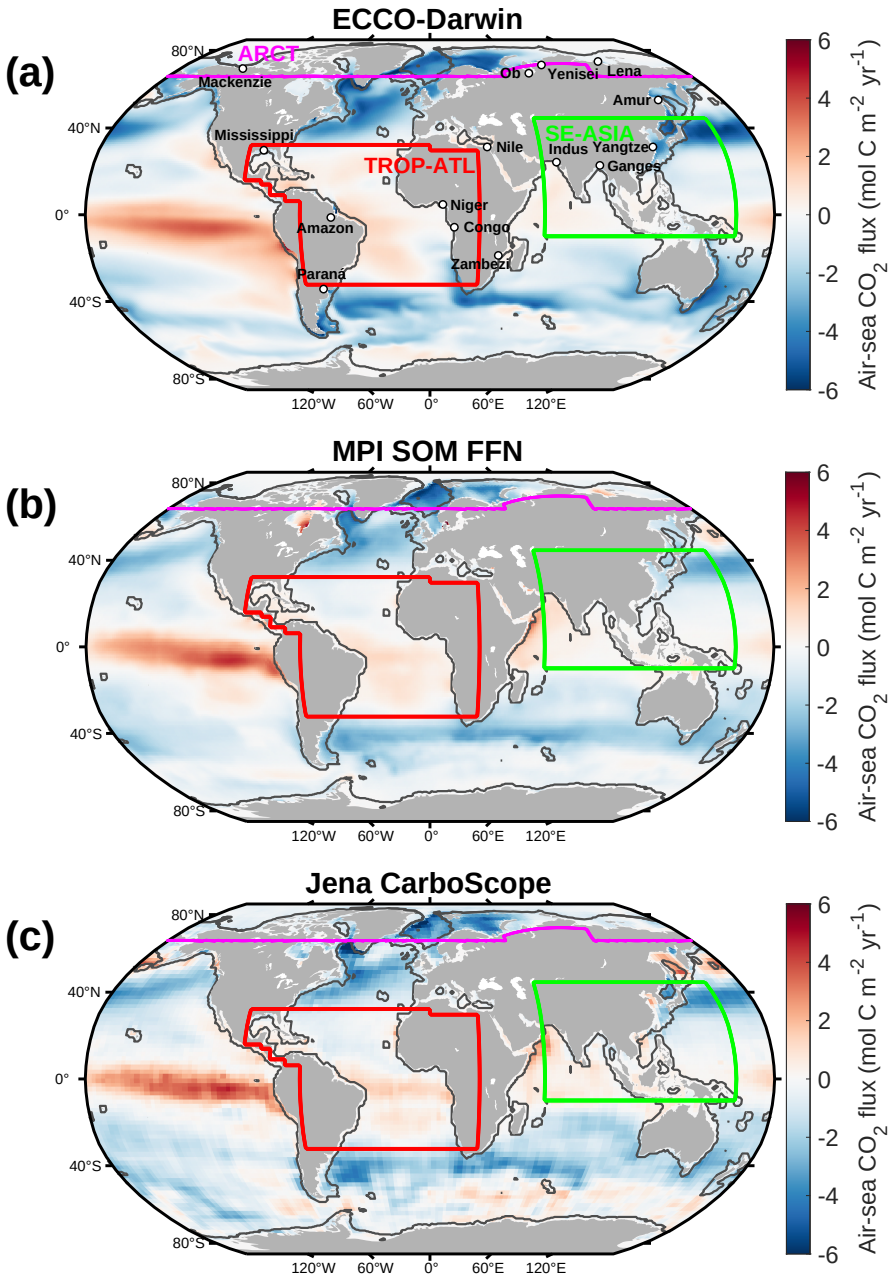

Figure 1. Climatological global-ocean air-sea CO_2 flux for (a) ECCO-Darwin Baseline, (b) MPI SOM FFN, and (c) Jena CarboScope. Positive values represent CO_2 outgassing (red colors); negative values are uptake (blue colors). All fields shown are time means from January 2000 to December 2019. Colored boundary lines correspond to domains used for regional analysis of the Arctic Ocean (ARCT, violet line), the Tropical Atlantic (TROP-ATL, red line), and Southeast Asia (SE-ASIA, green line). The black line delineates the coastal ocean from the open ocean, which is set by the furthest point from the coastline of either a 300-km distance or the 1000-m isobath. White points show river mouth locations for the top-15 global rivers in terms of watershed area. MPI SOM FFN v2022 and Jena CarboScope v2023 products were interpolated on the ECCO v4 LLC90 grid.

2.2 Biogeochemical River Runoff

In addition to the Baseline simulation, we conducted a suite of sensitivity experiments where we added terrestrial DOC (t_{DOC}), DIC (t_{DIC}), total alkalinity (t_{ALK}), dissolved inorganic nitrogen (t_{DIN}), dissolved organic nitrogen (t_{DON}), and dissolved silica (t_{DSi}), henceforth referred to as riverine exports in this study. We excluded phosphorus and iron due to the complexity of their reactions when entering the marine environment (i.e., absorption, bio-availability). Except for t_{DIC} and t_{ALK}, riverine exports are provided by the Global NEWS 2 (Global Nutrient Export from WaterSheds) model (Mayorga et al., 2010).

Global NEWS 2 uses statistical and mechanistic relations at the watershed scale to compute annual-mean freshwater discharge and riverine loads based on natural and anthropogenic sources, with 6292 individual watersheds delineated according to the global river systems dataset from Vörösmarty et al. (2000). t_{DIN} was partitioned into nitrite (NO_2^-), nitrate (NO_3^-), and ammonium (NH_4^+), according to the mean fraction of each species concentration relative to the total DIN concentration from the GLObal RIver CHemistry Database (GLORICH) (Hartmann et al., 2014). The NO_2^-:DIN, NO_3^-:DIN, and NH_4^+:DIN ratios were estimated to be 0.02, 0.65, and 0.33, respectively. Riverine t_{DIC} loads were computed using an empirical relation between freshwater discharge and gross CO_2 consumption from rock weathering as described in M. Li et al. (2017, equation 9). CO_2 consumption by rock weathering over each Global NEWS 2 watershed was estimated based on the freshwater discharge and the basin-dominant lithology (Amiotte Suchet et al., 2003). t_{ALK} loads were computed using an ALK:DIC ratio (0.98) based on the mean total ALK compared to DIC from GLORICH. t_{DOC} was not considered to be more refractory than marine DOC; the DOC remineralization rate is set to 1 over 100 days. We used Global NEWS 2 outputs for year 2000 as representative of present-day carbon and nutrient loads (Mayorga et al., 2010).

Global NEWS 2 river mouth locations were associated with JRA55-do grid points exhibiting the closest annual-mean freshwater discharge in 2000 within a euclidean distance of 5°. The top-100 largest rivers (by watershed extent) from Global NEWS 2 were imposed on JRA55-do grid points as a function of distance only. In total, 5171 river mouths were associated with JRA55-do grid points. For each discharge point, export concentrations from the associated river were estimated by dividing the load by the annual volume of freshwater from Global NEWS 2; the concentration was then converted to a daily flux using the corresponding daily-mean freshwater flux from JRA55-do. Exports were adjusted according to the grid cell area difference between JRA55-do and ECCO v4 LLC90. These biogeochemical exports were then added as point-source discharge along riverine freshwater flux (Figure 2). Due to extreme values in our automated Global-NEWS-2-derived computation for the Amazon River, the DIC load for this system was set to a more-realistic, literature-mean of 2.54 Tmol yr^{-1} (da Cunha & Buitenhuis, 2013; Probst et al., 1994; M. Li et al., 2017) (for more details see Supporting Information Text S1).

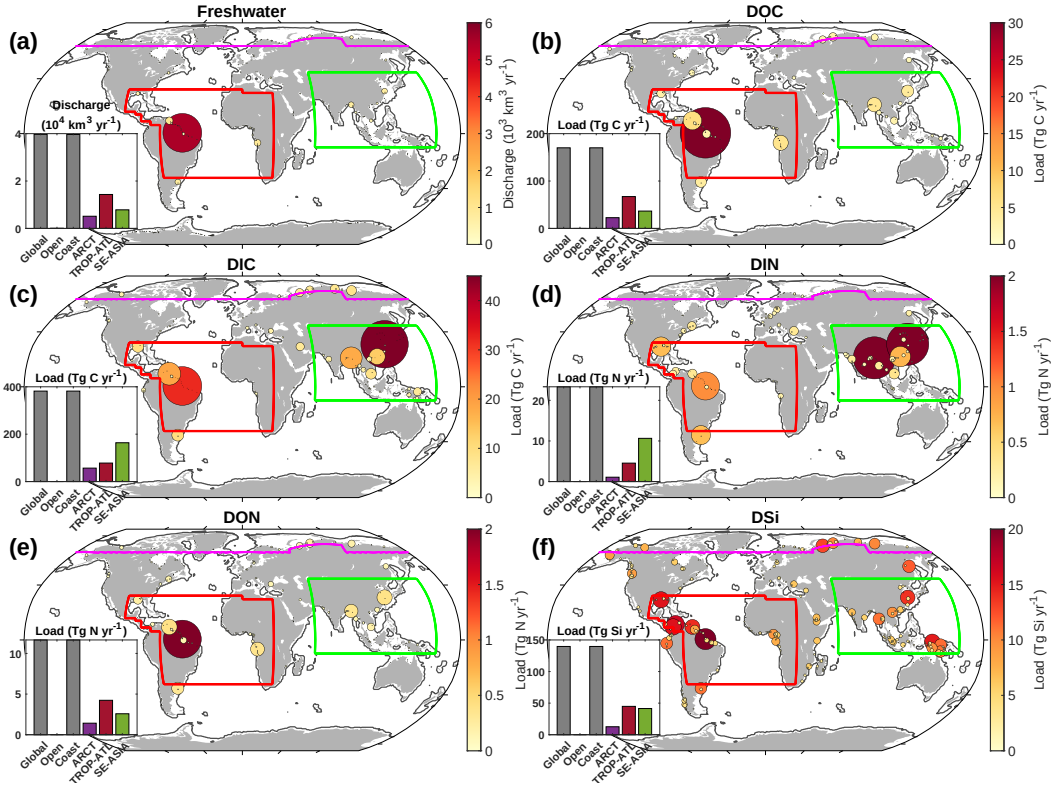

Figure 2. Riverine freshwater discharge and biogeochemical exports resulting from the association of Global NEWS 2 and JRA55-do on the ECCO v4 LLC90 grid. Domain-scale freshwater discharge and load is relative to the respective domain area. Insets show corresponding year-2000 discharge/load for various regions. The size of circles represents magnitude of loads. Colored boundaries correspond to domains used for regional analysis. The black line delineates the coastal ocean from the open ocean. Only rivers with annual discharge over 10 km^3 yr^{-1} are shown.

As riverine t_{DOC}, t_{DIN}, t_{DON}, and t_{DSi} were computed from Global NEWS 2 concentration and modulated with JRA55-do freshwater runoff, our fluxes agree well with existing estimates based on the NEWS 2 database (Mayorga et al., 2010; Frings et al., 2016; Sharples et al., 2017; Lacroix et al., 2020; Tivig et al., 2021; Tian et al., 2023). t_{DIC} lateral export from rivers was estimated according to Amiotte Suchet et al. (2003); Mayorga et al. (2010); M. Li et al. (2017), resulting in a t_{DIC} load of 381.81 Tg C yr^{-1} to the ocean, which is in general agreement with recent studies (Drake et al., 2018; M. Li et al., 2017; Lacroix et al., 2020; Battin et al., 2023; Tian et al., 2023).

2.3 Sensitivity Experiments and Analysis

Sensitivity experiments consisted of adding riverine exports separately or together along with freshwater runoff (Table 1). t_{ALK} was always added along with t_{DIC} in relevant experiments. Moreover, we ran additional sensitivity experiments using all riverine exports (Table 1, ALL_{run}) for each of the top-15 global rivers in terms of watersheds extent (Mayorga et al., 2010). Ancient river systems and rivers terminating in enclosed basins or on land were discarded from our analysis. The locations of the corresponding top-15 river mouths are shown in Figure 1.

Table 1. Annual carbon and nutrient loads in runoff sensitivity experiments.

Experiment Name	t_{DOC} (Tg C yr^{-1})	t_{DIC} (Tg C yr^{-1})	t_{DON} (Tg N yr^{-1})	t_{DIN} (Tg N yr^{-1})	t_{DSi} (Tg Si yr^{-1})
Baseline	0	0	0	0	0
DC_{run}	170.1	381.8	0	0	0
DIC_{run}	0	381.8	0	0	0
DN_{run}	0	0	11.7	23.3	0
DIN_{run}	0	0	0	23.3	0
DSi_{run}	0	0	0	0	139.7
ALL_{run}	170.1	381.8	11.7	23.3	139.7

We analyzed monthly-mean model fields along the coastal ocean (limits set by the furthest point from the coastline, either the 1000-m isobath or a distance of 300 km; 58 x 10^6 km^2) and the open ocean (300 x 10^6 km^2) during 2000–2019. In addition to the global ocean, we also evaluated the sensitivity of ocean carbon cycling in three specific regions that receive large volumes of freshwater from major river systems: the Arctic Ocean (ARCT, 22 x 10^6 km^2), Tropical Atlantic (TROP-ATL, 77 x 10^6 km^2), and Southeast Asia (SE-ASIA, 62 x 10^6 km^2). Coastal and open ocean boundaries are delineated by the black line in Figure 1. Monthly-mean net primary production (NPP) was integrated over the upper 100 m.

Furthermore, we separated the respective contributions of 1) the solubility pump and 2) primary production resulting from river-driven changes in climatological air-sea CO_2 flux (ΔCO_2) in the ALL_{run} as:

$$\Delta CO_2{}^{\mathrm{solub}^{C}} + \Delta CO_2{}^{\mathrm{solub}^{N,Si}} + \Delta CO_2{}^{\mathrm{NPP}^{N,Si}}, \tag{1}$$

where $\Delta CO_2{}^{\mathrm{solub}^{C}}$ and $\Delta CO_2{}^{\mathrm{solub}^{N,Si}}$ are the changes in air-sea CO_2 flux associated with the solubility pump due to the addition of terrestrial carbon and nitrogen/silica, respectively. $\Delta CO_2{}^{\mathrm{NPP}^{N,Si}}$ is the change in air-sea CO_2 flux driven by NPP in response to terrestrial nitrogen and silica.

In DC_{run}, changes in air-sea CO_2 flux are only associated with the solubility pump:

$$\Delta CO_2{}^{\mathrm{solub}^{C}} = \Delta CO_{2\,DC_{run}}. \tag{2}$$

We then associated the change in surface-ocean DIC concentration with ΔCO_2 driven by the solubility pump in DC_{run} to isolate ΔCO_2 due to the solubility pump relative to changes in surface-ocean DIC concentration in DN and DSi_{runs}:

$$\Delta CO_2{}^{\mathrm{solub}^{N,Si}} = \frac{\Delta CO_2{}^{\mathrm{solub}^{C}}}{[DIC]^{C}_{surf}} \times [DIC]^{N,Si}_{surf}. \tag{3}$$

The change in ΔCO_2 due to changes in NPP in DN and DSi_{runs} was then estimated by subtracting ΔCO_2 due to the solubility pump from the total ΔCO_2:

$$\Delta CO_2{}^{\mathrm{NPP}^{N,Si}} = \Delta CO_{2\,DN,DSi_{runs}} - \Delta CO_2{}^{\mathrm{solub}^{N,Si}}. \tag{4}$$

3 Results

3.1 Climatological Global Analysis

Along with 39,687 km^3 yr^{-1} of riverine freshwater, total loads of 551.9 Tg C yr^{-1}, 35 Tg N yr^{-1}, and 139.7 Tg Si yr^{-1} were exported into the global ocean in ALL_{run} (Table 1). The addition of dissolved carbon, nitrogen, and silica in ALL_{run} led to an increase in CO_2 outgassing of 0.03 Pg C yr^{-1} compared to the Baseline, globally (Figure 3a and Figure 4a, Table 2). The majority of CO_2 outgassing (0.04 Pg C yr^{-1}) occurs in the coastal ocean (Figure 3a and Table 2). In the open ocean, riverine exports slightly increased CO_2 uptake by 0.01 Pg C yr^{-1} (Figure 3a and Table 2).

In ALL_{run}, changes in air-sea CO_2 flux resulted from compensation between the effects of riverine carbon and nitrogen, as DC_{run} and DN_{run} experiments result in elevated CO_2 outgassing and uptake, respectively (Table 2). In DC_{run}, the increase in ocean carbon due to riverine exports diminished the ocean's capacity to take up atmospheric CO_2, resulting in a net CO_2 outgassing of 0.22 Pg C yr^{-1} (Table 2). In DN_{run}, the increase in nutrients to the euphotic zone led to increased phytoplankton productivity. The additional uptake of carbon by phytoplankton decreased surface-ocean DIC, resulting in an additional CO_2 sink of 0.17 Pg C yr^{-1} (Table 2).

CO_2 outgassing driven by riverine carbon (DC_{run}) was dominated by t_{DOC} (70%), with a smaller contribution from t_{DIC} (30%) (Figure 4a). While outgassing driven by riverine carbon was compensated by uptake due to nitrogen in the open ocean, CO_2 uptake due to nitrogen was 36% lower than riverine-carbon-driven coastal outgassing, leading to global-ocean net CO_2 outgassing in ALL_{run} (Table 2).

Riverine dissolved carbon, nitrogen, and silica also resulted in a NPP increase of 0.6 Pg C yr^{-1} (+2%) compared to Baseline (Figure 3b and Figure 4b, Table 2). Riverine t_{DIN} (DIN_{run}) contributed to 70% and 86% of the CO_2 uptake and NPP increase simulated in DN_{run}, respectively (Figure 4b). The total increase of NPP in ALL_{run} from riverine exports was equally distributed between the coastal and open ocean (0.3 Pg C yr^{-1} for each) (Figure 4b). However, the increase of NPP was stronger in the coastal ocean (+5.2 g C m^{-2} yr^{-1}, +7%) compared to the open ocean (+1 g C m^{-2} yr^{-1}, +1%) relative to their surface area.

Table 2. Air-sea CO_2 flux and NPP for each experiment in the coastal ocean, open ocean, and global ocean. Positive values represent CO_2 outgassing; negative values are uptake.

Domain	Experiment	CO_2 Flux (Pg C yr^{-1})	NPP (Pg C yr^{-1})
Coastal Ocean	Baseline	−0.68	3.8
	ALL_{run} − Baseline	+0.04	+0.3
	DC_{run} − Baseline	+0.1	0.0
	DN_{run} − Baseline	−0.07	+0.3
	DSi_{run} − Baseline	−0.01	+0.01
Open Ocean	Baseline	−1.90	20.6
	ALL_{run} − Baseline	−0.01	+0.3
	DC_{run} − Baseline	+0.1	0.0
	DN_{run} − Baseline	−0.1	+0.3
	DSi_{run} − Baseline	−0.01	+0.01
Global Ocean	Baseline	-2.58	24.4
	ALL_{run} − Baseline	+0.03	+0.6
	DC_{run} − Baseline	+0.22	0.0
	DN_{run} − Baseline	−0.17	+0.6
	DSi_{run} − Baseline	−0.01	+0.01

3.2 Climatological Regional Analysis

The Arctic Ocean region (Figure 1, ARCT) received 5,138 km^3 yr^{-1} of freshwater from rivers in Baseline, which is roughly 13% of global freshwater discharge. In ALL_{run}, freshwater discharge was supplemented with 22.6 and 56.8 Tg C yr^{-1} of t_{DOC} and t_{DIC}, respectively (Figure 2). The river load of carbon and t_{DOC} into ARCT represented 15% and 12% of their associated global loads, respectively. ARCT also received 2.5 Tg N yr^{-1} as t_{DON} (56%) and t_{DIN} (44%) in ALL_{run}. The t_{DSi} river load was 12.6 Tg Si yr^{-1} (Figure 2) in this region. Riverine export loads were primarily from the Ob, Yenisei, Lena, and Mackenzie Rivers (Figure 2 and Supporting Information Table S1).

In Baseline, ARCT produced a CO_2 uptake of roughly 0.21 Pg C yr^{-1}. When riverine carbon, nitrogen, and silica were added in ALL_{run}, ARCT CO_2 uptake was reduced by 0.02 Pg C yr^{-1}, with the majority of the response (80%) in the coastal ocean (Figure 3a and Figure 4a). Riverine-induced CO_2 outgassing was dominated by the input of t_{DOC} in ARCT (Figure 4a). 50% of the riverine-induced CO_2 outgassing was due to the Ob, Yenisei, Lena, and Mackenzie Rivers (Table 3). In the Baseline experiment, NPP was 0.22 Pg C yr^{-1}, with a similar magnitude in the coastal and open ocean. The addition of riverine nitrogen into ARCT increased coastal NPP by 40% (Figure 3b and Figure 4b).

The Tropical Atlantic (Figure 1, TROP-ATL) received 36% of global freshwater discharge (14,228 km^3 yr^{-1}) and 35% of the global t_{DOC} load from rivers (67.2 Tg C yr^{-1}). Combined with t_{DIC}, the net carbon load was 145.3 Tg C yr^{-1} (Figure 2). Roughly 30% of the global dissolved nitrogen and silica river load was delivered to TROP-ATL, with river loads dominated by the Amazon River (Figure 2 and Supporting Information Table S1).

Riverine carbon, nitrogen, and silica resulted in a TROP-ATL CO_2 outgassing of 0.02 Pg C yr^{-1} compared to Baseline (0.10 Pg C yr^{-1}). This imbalance resulted from CO_2 outgassing driven by carbon, which was 30% larger than uptake due to increased phytoplankton productivity from riverine nitrogen (Figure 4a). 85% of CO_2 outgassing in DC_{run} was driven by riverine t_{DOC} (Figure 4a). Riverine t_{DOC} indirectly drives CO_2 outgassing by first being remineralized to DIC, which increases DIC concentration in the ocean and thus limits the ocean's capacity to take up atmospheric CO_2. Most of the CO_2 outgassing driven by t_{DOC} occurs in the open ocean (Figure 3a and Figure 4a). The Amazon River drove 70% of riverine-induced CO_2 outgassing in TROP-ATL (Table 3). In Baseline, NPP in TROP-ATL was 3.18 Pg C yr^{-1}. The increase in NPP driven by riverine t_{DIN} occurred predominantly in the open ocean (∼60%) compared to the coastal (∼40%) zone (Figure 4b). The Amazon River was responsible for 65% of the NPP increase driven by riverine exports (Figure 4b).

In Baseline, the freshwater discharge into SE-ASIA was 7,841 km^3 yr^{-1}, roughly 20% of global discharge. In ALL_{run}, SE-ASIA received 38% of dissolved carbon from rivers, globally (207.39 Tg C yr^{-1}). 81% of dissolved carbon delivered into SE-ASIA was inorganic, representing 42% of the global t_{DIC} river load (Figure 2). SE-ASIA also received 45% (10.6 Tg N yr^{-1}) of the global t_{DIN} load from rivers (Figure 2). 41.5 Tg Si yr^{-1} was discharged into SE-ASIA (Figure 2). Nutrient loads into SE-ASIA were dominated by high riverine t_{DIC} and t_{DIN} from the Ganges and Yangtze Rivers (Figure 2 and Supporting Information Table S1). The Yangtze river contributed 12% of t_{DIC} river loads, globally (Figure 2 and Supporting Information Table S1). Taken together, the Yangtze and Ganges Rivers delivered 20% of the global t_{DIN} river load (Figure 2 and Supporting Information Table S1).

SE-ASIA had a CO_2 sink of 0.30 Pg C yr^{-1} in Baseline, while CO_2 uptake increased by 0.02 Pg C yr^{-1} in ALL_{run} (Figure 4a). Riverine carbon- and nitrogen-driven air-sea CO_2 flux was compensated in the coastal ocean (±0.03 Pg C yr^{-1}). However, in the open ocean, the riverine nitrogen-driven increase in NPP and associated CO_2 uptake was two times higher than carbon-driven outgassing — leading to an overall imbalance and resulting in net CO_2 uptake in the domain (Figure 4a).

t_{DIN} was responsible for 85% of biological CO_2 uptake (Figure 4a). The Ganges River (58%), combined with the Indus and Yangtze Rivers, were responsible for 77% of CO_2 uptake in SE-ASIA (Table 3). NPP in SE-ASIA without the addition of riverine exports was 3.3 Pg C yr^{-1}. In ALL_{run}, NPP increased by 0.30 Pg C yr^{-1} due to elevated t_{DIN} in both the open and coastal ocean (Figure 4b). The Ganges and Yangtze Rivers caused roughly 40% of the NPP increase in SE-ASIA (Table 3).

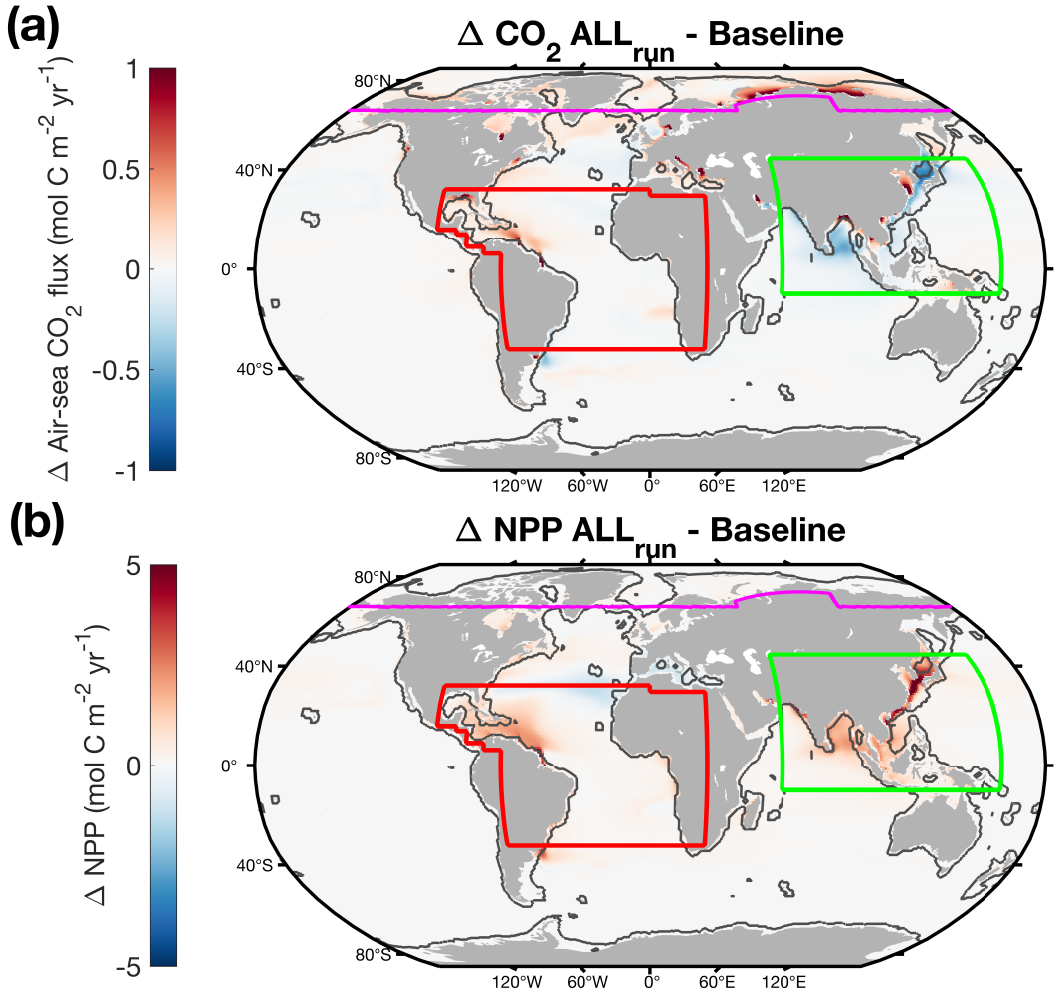

Figure 3. Global-ocean (a) air-sea CO_2 flux and (b) NPP driven by riverine exports in ALL_{run}. Fields represent time-mean values from January 2000 to December 2019. Colored lines on maps show domains used for regional analysis. The black line delineates the coastal ocean from the open ocean.

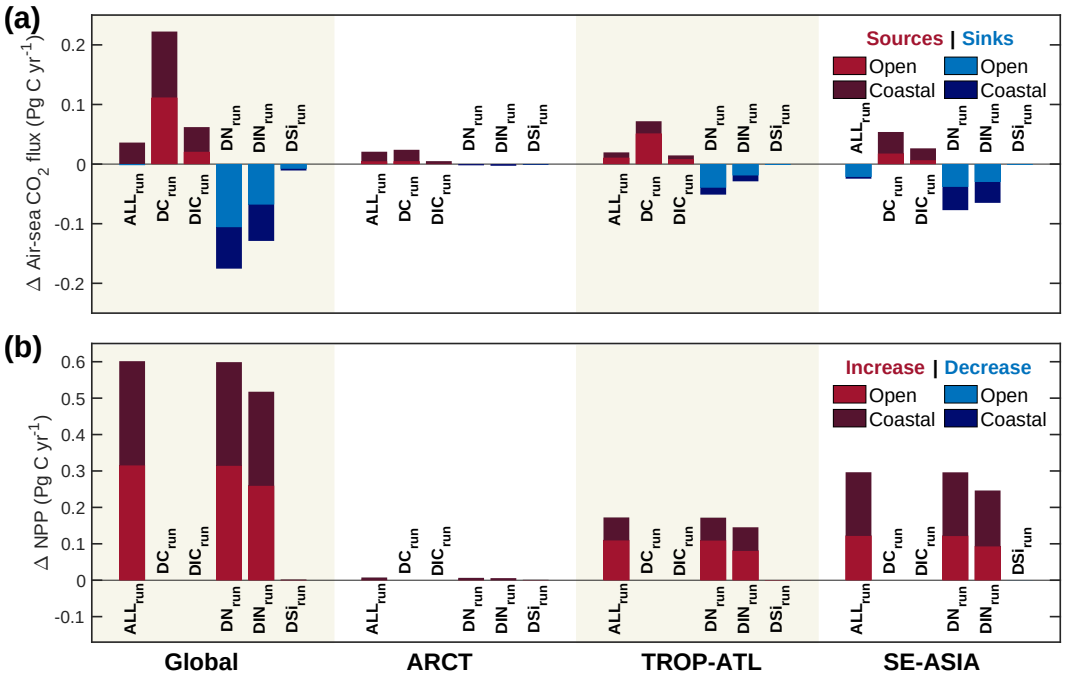

Figure 4. Domain-integrated differences in (a) air-sea CO_2 flux and (b) NPP driven by riverine exports in each sensitivity experiment. Differences were computed from time-mean fields from January 2000 to December 2019. The black line delineates the coastal ocean from the open ocean.

Table 3. Contribution of the global top-15 rivers in terms of watershed area to changes in air-sea CO_2 flux and NPP. Positive values represent CO_2 outgassing driven by the corresponding river; negative values are uptake. The respective river contribution is estimated from the difference between Baseline and a modified ALL_{run}, where only the corresponding river was included. Locations of river mouths are shown in Figure 1.

Rank	River	Δ CO_2 Flux (Tg C yr^{-1})	Δ NPP (Tg C yr^{-1})
1	Amazon	+14.3	+113.6
2	Nile	+0.3	-0.1
3	Congo	+1.3	+12.4
4	Mississippi	-1.3	+26.4
5	Ob	+2	+2.2
6	Paraná	+0.5	+13.5
7	Yenisei	+2.6	+1.5
8	Lena	+2.8	+1.1
9	Niger	-0.1	+3
10	Yangtze	-3	+57.3
11	Amur	+0.7	+1.7
12	Mackenzie	+1.7	+0.6
13	Ganges	-11.7	+64.5
14	Zambezi	+0.1	+1
15	Indus	-0.7	+3.7
N/A	Total	+9.5	+302.4

3.3 Mechanisms of River-driven Air-sea CO_2 Flux

From January 2000 to December 2019, the time-mean surface-ocean DIC mass in DC_{run} increased by 370.7 Tg C. This triggered a solubility-pump-driven outgassing of 222.4 Tg C yr^{-1} (Figure 4a). Over the same period, the addition of terrestrial nitrogen and silica, the sum of DN_{run} and DSi_{run}, drove a reduction of 21.5 Tg C in the surface-ocean DIC mass. Assuming the same ratio of surface-ocean DIC and air-sea CO_2 flux as in DC_{run}, the input of terrestrial nitrogen and silica will cause a CO_2 uptake of 12.9 Tg C yr^{-1} (Figure 4b). Since the net ocean CO_2 uptake increased by 186.2 Tg C yr^{-1} in response to terrestrial nitrogen and silica fertilization of NPP, the net increase in global CO_2 uptake is 173.3 Tg C yr^{-1} (Figure 4c).

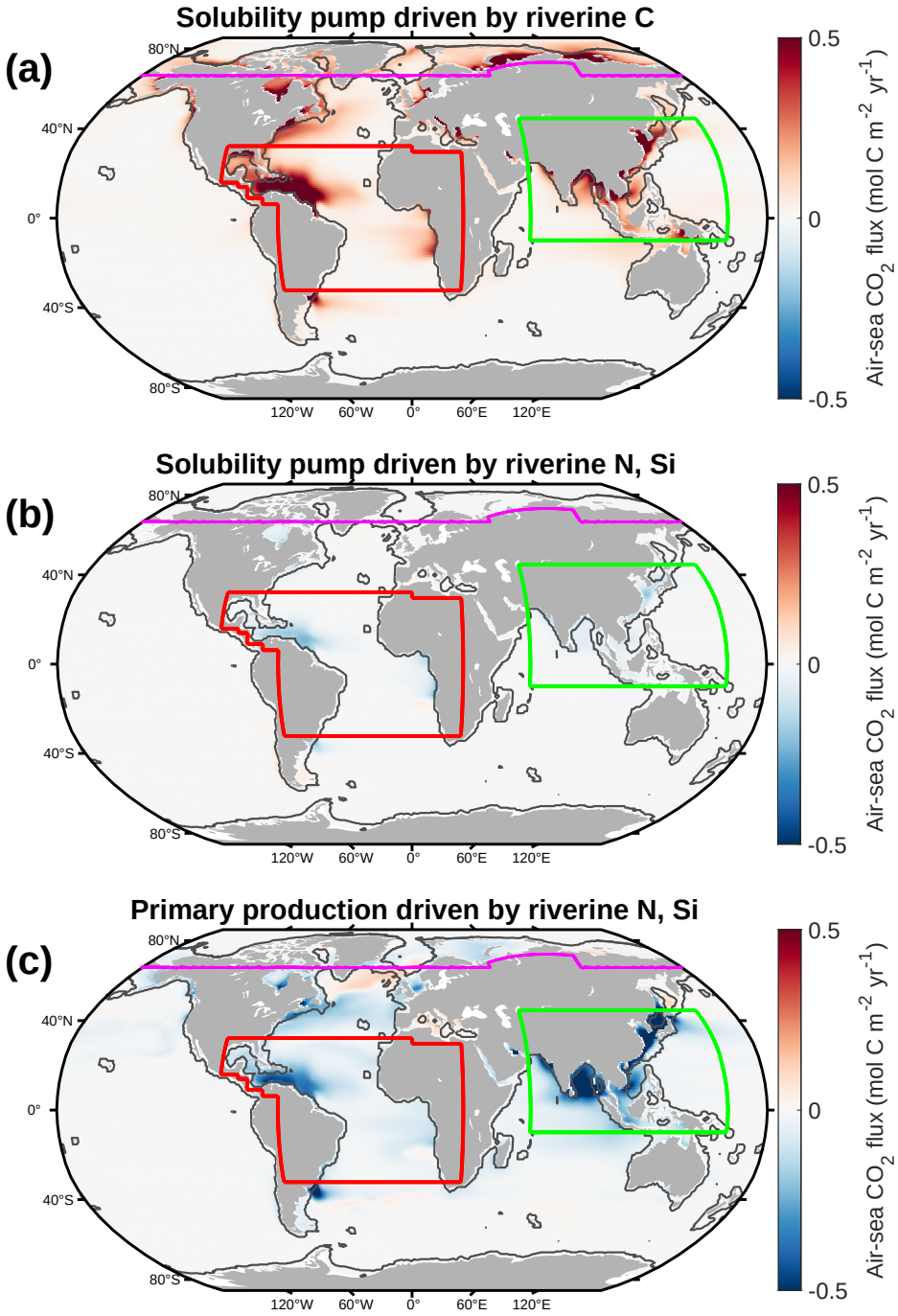

Figure 5. Climatological (January 2000 to December 2019) air-sea CO_2 flux CO_2associated with (a) change in the solubility pump driven by riverine carbon, (b) change in the solubility pump driven by riverine nitrogen and silica, and (c) NPP driven by riverine nitrogen and silica. Colored lines on maps show domains used for regional analysis. The black line delineates the coastal ocean from the open ocean.

Overall, the change in air-sea CO_2 flux driven by riverine exports was dominated 1) by the solubility pump near river mouths in response to terrestrial carbon and 2) by NPP in the open ocean where CO_2 uptake from nitrogen- and silica-driven phytoplankton blooms exceeded riverine carbon-driven outgassing (Figure 4 and Figure 6). TROP-ATL and ARCT were dominated by riverine-driven CO_2 outgassing (71.9 and 24 Tg C yr^{-1}, respectively) and CO_2 uptake due to NPP fertilization in TROP-ATL and ARCT was minor (44.4 and 3.3 Tg C yr^{-1}, respectively). In SE-ASIA, the increase of CO_2 uptake due to enhanced NPP (69.6 Tg C yr^{-1}) exceeded CO_2 outgassing driven by riverine carbon (53.9 Tg C yr^{-1}).

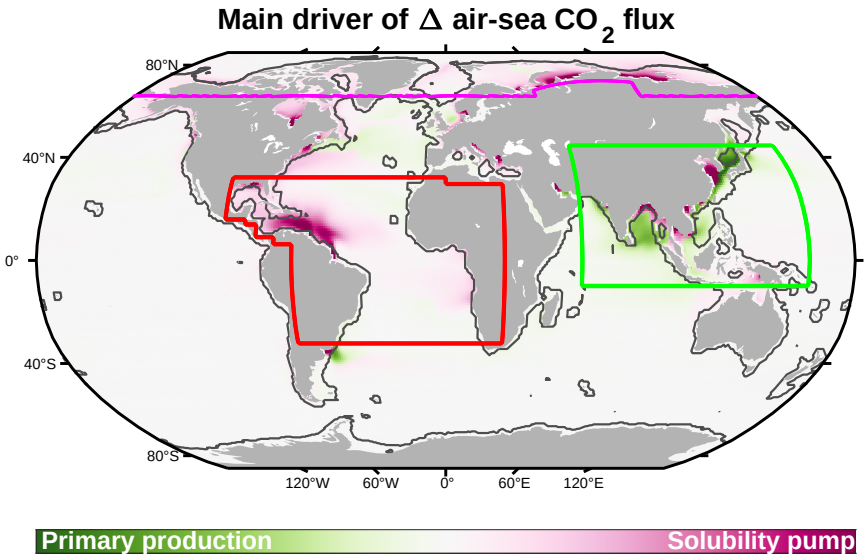

Figure 6. Pathways of change in climatological (January 2000 to December 2019) air-sea CO_2 flux driven by riverine exports. Colors represent the dominant flux shown in Figure 4. The black line delineates the coastal ocean from the open ocean.

4 Discussion

4.1 Fate of Riverine Dissolved Carbon and Nutrients

Once in the ocean, terrestrial dissolved carbon (t_{DOC} and t_{DIC}) result in a source of CO_2 to the atmosphere through a reduction of the solubility pump (Figure 7). Terrestrial nutrients, such as nitrogen and silica (t_{DIN}, and t_{DSi}), fertilize phytoplankton and elevate CO_2 uptake via increased NPP.

The resultant export of marine organic carbon (m_{OC}) from the surface ocean drives additional CO_2 uptake via the solubility pump; at depth, the exported m_{OC} is remineralized to inorganic carbon (m_{IC}) (Figures 4b and 7). Thus, terrestrial nutrients have the

potential to shift riverine carbon-driven CO_2 outgassing to uptake, due to assimilation of carbon by primary producers. Despite a stronger increase of NPP in the coastal ocean (+5.2 g C m^{-2} yr^{-1}, +7%) compared to the open ocean (+1 g C m^{-2} yr^{-1}, +1%), the outgassing of CO_2 driven by riverine carbon through the solubility pump dominates changes in air-sea CO_2 flux close to river mouths. In contrast, the riverine nitrogen and silica signal spreads further offshore and enhances NPP and CO_2 uptake — this mechanism dominates the change in air-sea CO_2 flux in open-ocean regions.

In carbon-dominated terrestrial margins, such as TROP-ATL and ARCT, rivers drive a large source of CO_2 from the ocean to the atmosphere. However, in nitrogen-dominated margins, such as SE-ASIA, the addition of lateral fluxes drives a substantial ocean carbon sink. Globally, these two processes tend to compensate each other and our simulations suggest that the addition of riverine dissolved carbon, nitrogen, and silica result in a small net source of atmospheric CO_2in the global ocean.

Table 4. Riverine exports loads.

Domain	Export (Tg yr^{-1})	ALL_{run}	Literature Value
Global	t_{DOC}	170.1	130–262 [1]
	t_{DIC}	381.8	320–453 [1]
	t_{DON}	11.7	11.8 [1]
	t_{DIN}	23.3	17–22.8 [1]
	t_{DSi}	139.7	158–171 [1]
ARCT	t_{DOC}	22.6	34–37.7 [2]
	t_{DIC}	56.8	57 [2]
	t_{DON}	1.4	0.05–0.84 [2]
	t_{DIN}	1.1	0.04–0.43 [2]
	t_{DSi}	12.6	11.4 [2]
TROP-ATL	t_{DOC}	67.2	46 [3]
	t_{DIC}	78.1	50 [3]
	t_{DON}	4.2	N/A
	t_{DIN}	4.5	15.3 [3]
	t_{DSi}	44.9	53 [3]
SE-ASIA	t_{DOC}	36.6	N/A
	t_{DIC}	163.8	40 [4]
	t_{DON}	2.6	N/A
	t_{DIN}	10.6	2.1–8.4 [4*]
	t_{DSi}	41.5	N/A

[1] (Drake et al., 2018; Mayorga et al., 2010; Frings et al., 2016; Sharples et al., 2017; Lacroix et al., 2020; Tivig et al., 2021; Tian et al., 2023; M. Li et al., 2017; Lacroix et al., 2020; Battin et al., 2023; Tian et al., 2023)
[2] (Manizza et al., 2011; Tank et al., 2012; Holmes et al., 2012; Le Fouest et al., 2013)
[3] (Cotrim da Cunha et al., 2007; Araujo et al., 2014)
[4] (Singh & Ramesh, 2011; H.-M. Li et al., 2014; J. Wang et al., 2020; Nishina et al., 2021; Piao et al., 2012; Patra et al., 2013)
[*] Computed from the sum of regional estimates

Table 5. Change in air-sea CO_2 flux and NPP driven by riverine exports.

Domain	ΔCO_2/NPP	ALL_{run} (Pg C yr^{-1})	Literature Value (Pg C yr^{-1})
Global	Δ CO_2	+0.03	+0.11 [1]
	Δ NPP	+0.6	+0.6–3.9 [1]
ARCT	Δ CO_2	+22.8	+0.6–20 [2*]
	Δ NPP	+7.4	+58 [2]
TROP-ATL	Δ CO_2	+20	+5–20 [3**]
	Δ NPP	+170	+80–400 [3]
SE-ASIA	Δ CO_2	-24.7	N/A
	Δ NPP	+296	+100 [4]

[1] (Tivig et al., 2021; Cotrim da Cunha et al., 2007)
[2] (Manizza et al., 2011; Terhaar et al., 2021)
[3] (da Cunha & Buitenhuis, 2013; Louchard et al., 2021)
[4] (Tivig et al., 2021)
[*] Effect of t_{DOC} only
[**] Lower bound is for smaller domain in western TROP-ATL

For both Baseline and ALL_{run}, the ocean CO_2 sink (2.55–2.58 Pg C yr^{-1}) lies within the range of recent estimates (Resplandy et al., 2018; Regnier et al., 2022; Friedlingstein et al., 2023). This present-day ocean CO_2 sink reflects the contribution of climate and anthropogenic perturbations on top of preindustrial levels. In this study, a net riverine carbon export of 0.55 Pg C yr^{-1} (Table 1, t_{DOC} + t_{DIC}) drives a CO_2 outgassing of 0.22 Pg C yr^{-1}, while 35 Tg N yr^{-1} (Table 1, t_{DON} + t_{DIN}) drives a CO_2 uptake of 0.17 Pg C yr^{-1} from enhanced ocean fertilization. We note that our multi-decadal estimates are not in steady state and do have a realistic representation of estuarine, blue carbon, and bottom sediment processes. Therefore, they are not directly comparable to steady-state, pre-industrial estimates of the river loop (Resplandy et al., 2018).

The introduction of terrestrial nutrients, such as inorganic nitrogen and silica, increased global-ocean marine NPP by 0.6 Pg C yr^{-1} compared to Baseline. The addition of t_{DIN} and t_{DON} also increased ocean NPP by 0.6 Pg C yr^{-1} in the model described in Tivig et al. (2021) (Table 5). The modeling study by Lacroix et al. (2020) also depicted a 3% increase of ocean NPP in response to the addition of riverine nutrients. In our study, the increase of NPP driven by riverine exports was stronger in the coastal ocean compared to the open ocean, relative to their respective surface areas. This is consistent with the recent study of Mathis et al. (2024), which demonstrates the role of increased riverine nutrient loads in driving stronger biological carbon fixation and thus an enhanced CO_2 sink in the coastal ocean during the last century.

4.2 Spatial Variability

In this section, we analyze the impact of riverine exports on the spatial variability of the ocean carbon cycle for our three regions of interest: ARCT, TROP-ATL, and SE-ASIA.

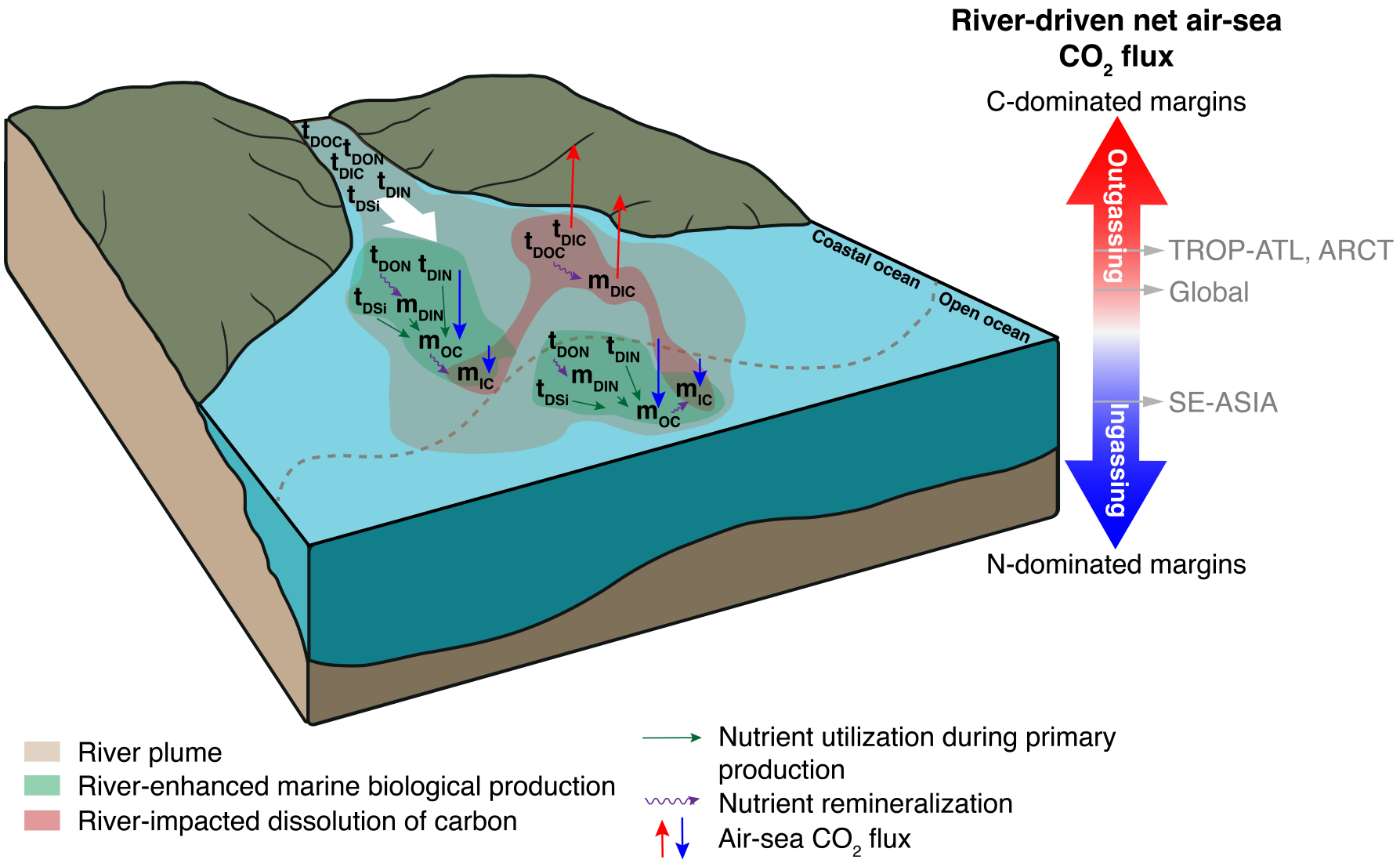

Figure 7. Fate of riverine exports in the coastal and open ocean. t_{DOC}: terrestrial DOC, t_{DIC}: terrestrial DIC, t_{DON}: terrestrial DON, t_{DIN}: terrestrial DIN, t_{DSi}: terrestrial DSi, m_{DIN}: marine DIN, m_{IC}: marine inorganic carbon, and m_{OC}: marine organic carbon. The dashed grey line delineates the coastal ocean from the open ocean.

manuscript submitted to *Global Biogeochemical Cycles*

4.2.1 Arctic Ocean (ARCT)

In the present study, the amount of freshwater, t_{DIC}, t_{DOC}, t_{DON}, t_{DIN}, and t_{DSi} delivered to the ARCT by individual rivers (Yenisey, Lena, Ob, and Mackenzie) falls within the range of observations from Tank et al. (2012), Le Fouest et al. (2013), and Holmes et al. (2012) (Supporting Information Table S1); suggesting that our estimates are reliable at the pan-Arctic scale (Table 4). In Baseline, ARCT uptakes 213.9 Tg C yr^{-1} of atmospheric CO_2.The addition of riverine exports reduces this CO_2 sink by 20 Tg C yr^{-1} and results in ECCO-Darwin having a more-consistent Arctic Ocean sink compared to previous studies (Manizza et al., 2011; Mortenson et al., 2020). In this region, riverine carbon dominates the response of air-sea CO_2 flux, with riverine t_{DOC} being responsible of 80% of CO_2 outgassing in ARCT. In Bertin et al. (2023), riverine exports from the Mackenzie River drove a CO_2 outgassing of roughly 0.5 Tg C yr^{-1} in the river plume. Our model depicts a CO_2 outgassing of similar magnitude in the river plume region ($\sim$0.1 Tg C yr^{-1}).

Due to anthropogenic climate change, thawing of carbon-rich permafrost is supplementing the load of t_{DOC} into Arctic rivers (Spencer et al., 2015). Permafrost-derived DOC has a relatively fast remineralization rate ($\sim$ 2 weeks) that could lead to strong CO_2 outgassing along coastal Arctic margins, which are dominated by permafrost-covered watersheds (Bertin et al., 2023). Furthermore, the degradation of organic carbon by microbial activity may be enhanced by changes in environmental conditions, such as increasing sea-surface temperature in ARCT (Carvalho & Wang, 2020). This would likely increase ocean CO_2 outgassing in response to the riverine carbon depicted in our study. Additionally, riverine nutrients also contribute to the Arctic Ocean carbon sink as they fertilize coastal waters. NPP in the Arctic Ocean increased by 3% (+7.4 Tg C yr^{-1}) in ALL_{run} compared to Baseline. However, recent estimates by Terhaar et al. (2021) suggests that riverine nutrients support up to 9–11% (+58 Tg C yr^{-1}) of marine NPP in the ARCT, in agreement with estimates by (Le Fouest et al., 2013, 2015) (Table 5). Therefore, CO_2 uptake driven by ocean fertilization from riverine nitrogen, and its capacity to compensate CO_2 outgassing in ARCT, might be underestimated in our study.

4.2.2 Tropical Atlantic (TROP-ATL)

Four of the top-15 global largest rivers (Amazon, Congo, Mississippi, and Niger) discharge into TROP-ATL. In total, rivers carry 67.2 Tg C yr^{-1} as t_{DOC}, 78.1 Tg C yr^{-1} as t_{DIC}, 4.2 Tg N yr^{-1} as t_{DON}, 4.5 Tg N yr^{-1} as t_{DIN}, and 44.9 Tg Si yr^{-1} as t_{DSi} into TROP-ATL. Riverine t_{DOC}, t_{DIC}, and silica loads in our study are consistent with estimates from Cotrim da Cunha et al. (2007) and Araujo et al. (2014) (46 and $\sim$50 Tg C yr^{-1} and 53 Tg Si yr^{-1}, respectively; Table 4). Our estimate of t_{DIN} delivered to this region is 3-fold lower than the value of 15.3 Tg N yr^{-1} reported by Cotrim da Cunha et al. (2007) (Table 4). However, t_{DIN} export from the Amazon river (1 Tg N yr^{-1}) agrees well with Louchard et al. (2021) (0.9 Tg N yr^{-1}). A dynamic land ecosystem model that explicitly resolves fluxes over the entire watershed estimated that 0.9 Tg N yr^{-1} is exported as t_{DIN} from the Mississippi River (Tian et al., 2020), which is in general agreement with the 0.7 Tg N yr^{-1} that we use as input for our model. The load of t_{DIN} from the Congo River (0.2 Tg N yr^{-1}) is also the same order of magnitude compared to data from Jouanno et al. (2021). However, our Global-NEWS-2-based estimate of 0.1 Tg N yr^{-1} remains lower than previous estimates for the Niger River (Robertson & Rosswall, 1986) (0.5 Tg N yr^{-1}). We stress that in Africa river systems, nutrient loads are poorly constrained due to sparse data.

In Baseline, TROP-ATL is a source of CO_2 to the atmosphere (0.10 Pg C yr^{-1}), which agrees with both interpolation-based products (Landschützer et al., 2016; Jersild et al., 2023; Rödenbeck, 2005) (0.04–0.08 Pg C yr^{-1}) and model results (da Cunha & Buitenhuis, 2013; Louchard et al., 2021) (0.03–0.04 Pg C yr^{-1}). We note that previous

studies show a river-driven increase in CO_2 uptake of 0.005 and 0.02 Pg C yr^{-1} when adding biogeochemical runoff in TROP-ATL and western TROP-ATL, respectively (da Cunha & Buitenhuis, 2013; Louchard et al., 2021). However, in our simulations, the addition of riverine exports in ALL_{run} enhanced the source of CO_2 (+0.02 Pg C yr^{-1}) (Table 5).

Contrary to the estimates of Louchard et al. (2021), which include physical effects associated with freshwater, such as enhanced upper-ocean stratification and gas solubility, our baseline simulation already includes these processes. Therefore, our suite of experiments cannot isolate and quantify the impact of freshwater discharge on ocean biogeochemistry. Freshwater in river plumes facilitates the uptake of atmospheric CO_2 through the solubility pump, which in turn overlaps with the sink of CO_2 associated with biogeochemical runoff. In addition to nitrogen, Louchard et al. (2021) also included inorganic phosphorus loads and a regionally-adjusted plankton ecosystem, e.g., by including a nitrogen-fixing phytoplankton functional type, which increased the model's capability to better resolve the biological pump and hence CO_2 uptake. For our simulations, we find that the increase of NPP associated with rivers in TROP-ATL (0.17 Pg C yr^{-1}) lies within the value of 0.08 Pg C yr^{-1} reported in Louchard et al. (2021) (Table 5) and the value of 0.4 Pg C yr^{-1} reported in Cotrim da Cunha et al. (2007). We note that horizontal resolution is also important for realistic representation of coastal processes. In their higher-resolution study, Louchard et al. (2021) were able to separately resolve the estuarine and plume/shelf waters of the Amazon River as a CO_2 source and sink, respectively, whereas our model intrinsically lacks such fine delineation.

The Amazon River clearly dominates the CO_2 outgassing signal in TROP-ATL, which is driven by the large load of t_{DOC}. Along with other rivers such as the Congo, Niger, and Orinoco Rivers, the Amazon River delivers a large amount of t_{DOC}, which originates from tropical forests. These forests contribute roughly one third of terrestrial NPP and their soil contains large amount of organic carbon, globally (Cleveland et al., 2010). As these watersheds are being drained by runoff from high precipitation, the subsequent high discharge, combined with carbon-rich soil and vegetation, leads to routing of t_{DOC}-rich waters to the coastal ocean (M. Li et al., 2019). At present time, it is critical to better constrain export of carbon from watersheds to coastal waters and characterize their fate in the ocean, as current efforts may be overestimating the land sink of carbon associated with tropical forests (Lauerwald et al., 2020). Additionally, the composition (refractory black carbon from combustion) and the quantity (CO_2 fertilization from NPP and soil erosion with deforestation) of carbon exports from the Amazon River remains uncertain due to ongoing changes in regional climate and fire regimes (Fleischer et al., 2019; Jones et al., 2020; Riquetti et al., 2023).

4.2.3 Southeast Asia (SE-ASIA)

Riverine biogeochemical runoff in SE-ASIA is dominated by high loads of t_{DIN} (10.6 Tg N yr^{-1}) and t_{DIC} (163.8 Tg C yr^{-1}), especially from the Ganges and Yangtze Rivers. The magnitude of the riverine t_{DIN} load for SE-ASIA compares with individual estimates for the Bay of Bengal (0.4 Tg N yr^{-1}), the Arabian Sea (0.06 Tg N yr^{-1}), and the East China Sea (1.6–7.9 Tg N yr^{-1}) (Singh & Ramesh, 2011; H.-M. Li et al., 2014; J. Wang et al., 2020; Nishina et al., 2021) (Table 4). Our estimate of the t_{DIC} load in SE-ASIA remains higher than values reported in the literature ($\sim$ 40 Tg C yr^{-1}) (Piao et al., 2012; Patra et al., 2013) and thus would require a regional adjustment as we did for the Amazon River (Table 4 and Supporting Information Text S1). This is explained by overestimated t_{DIC} loads from the Yangtze (45.9 Tg yr^{-1}) and the Ganges (18 Tg yr^{-1}) Rivers compared to reported values (20 and 3–4 Tg C yr^{-1}, respectively) (F. Wang et al., 2007; Guo et al., 2015; Y. Gao et al., 2017; Samanta et al., 2015). This overestimation is related to the relationship based on river discharge and the dominant lithology (Amiotte Suchet et al., 2003; M. Li et al., 2017). Both rivers exhibit high discharge combined with weathering-

prone lithologies (carbonate rocks and shales for the Yangtze and Ganges rivers, respectively), which consume atmospheric CO_2 due to high rates of rock weathering (Amiotte Suchet et al., 2003). The Yangtze River is also known for its high river CO_2 emission flux due to the large permafrost area in the Qinghai-Tibet Plateau that releases large DIC loads during warm and rainy summer conditions (Song et al., 2020). As for ARCT, the t_{DIC} load from the Yangtze watershed remains uncertain, as its permafrost region is degrading quickly under the effect of climate warming (Cheng & Wu, 2007; Yang et al., 2010).

Similar to ARCT, SE-ASIA is a sink of atmospheric CO_2 in Baseline (0.3 Pg C yr^{-1}). Combining air-sea CO_2 budgets for the different regions composing SE-ASIA from literature (East-Pacific, Indonesian seas, and North Indian Ocean without including Oman and Somalian upwelling regions), we estimate a carbon sink of ∼0.2 Pg C yr^{-1} for the entire SE-ASIA domain (Kartadikaria et al., 2015; De Verneil et al., 2021; Zhong et al., 2022; Hood et al., 2023). Our study provides the first estimate of the contribution of present-day riverine exports to the carbon sink in SE-ASIA. The net air-sea CO_2 exchange balance driven by riverine exports in SE-ASIA results in a carbon sink of 0.02 Pg C yr^{-1} in ALL_{run}. Compared to ARCT and TROP-ATL, carbon uptake in SE-ASIA is enhanced by a strong increase in marine NPP (+0.30 Pg C yr^{-1}, +9%) driven by riverine t_{DIN}. In Tivig et al. (2021), the simulated increase of NPP in response to riverine nitrogen was roughly 0.1 Pg C yr^{-1} in Asia, with the strongest increase in the Yellow Sea, similar to our results (Table 5). Riverine nitrogen loads in this domain, and especially in the China seas, have been supplemented by increased nitrogen deposition, nitrogen fertilizer, manure, and human sewage over the last 50 years (Nishina et al., 2021). Even if nitrogen runoff is declining, agricultural-driven nitrogen loads will remain at significant levels and continue to fertilize phytoplankton blooms in this nitrogen-depleted marine region due to high denitrification (Michael Beman et al., 2005; Nishina et al., 2021). Locally, the addition of riverine biogeochemical runoff also drives a source of CO_2 to the atmosphere, which is primarily limited to near river mouth locations in SE-ASIA. In the Yellow Sea and the Northern Bay of Bengal, close to the Yangtze and Ganges Rivers, the addition of riverine exports at preindustrial levels in an ocean model also drove a CO_2 outgassing in Lacroix et al. (2020). Noticeably, in our simulations, riverine carbon turns the northern Bay of Bengal into a carbon source as suggested by Hood et al. (2023).

4.3 Model Improvements

Our study is a first attempt to add global, time-varying biogeochemical discharge in the ECCO-Darwin ocean carbon estimation framework. Here, we elaborate on some necessary, and potentially consequential, simplifications made in this study. In light of these simplifications, some next-step model improvements are described in Supporting Information Text S2.

Rivers are a significant source of phosphorus and iron that is pivotal for ocean biogeochemistry (Krachler et al., 2005; Tagliabue et al., 2017; Duhamel et al., 2021; Savenko & Savenko, 2021). Consequently, our results may underestimate the global-ocean air-sea CO_2 uptake due to the absence of riverine phosphorus or iron in the model, as they might be limiting for ocean NPP relative to the excess of terrestrial inorganic nitrogen. Additionally, riverine t_{ALK} flux was computed based on a constant ALK:DIC ratio, globally (0.98). We note that the GLORICH database used to compute the mean ALK:DIC ratio has relatively good coverage over the American continent but Eurasia and Africa are underrepresented (Hartmann et al., 2014). As such, the ALK:DIC ratio can vary substantially over regional scales. The lack of this spatially-granular information in our simulated exports may misrepresent riverine t_{ALK} fluxes and the alkalinity-driven buffering capacity of simulated river plumes (Dubois et al., 2010; Tank et al., 2012; Mol et al., 2018; Ghosh et al., 2021; Gomez et al., 2023). While in estuaries the absence of ALK relative to DIC leads to higher partial pressure of CO_2 (pCO_2) in upper-ocean waters and enhanced CO_2 outgassing, rivers also bring an excess of ALK relative to DIC on con-

tinental shelves, which can reduce ocean pCO_2 through buffering and thus facilitate CO_2 uptake (W.-J. Cai et al., 2010; Louchard et al., 2021). Furthermore, the fate of riverine t_{ALK} in the ocean is associated with the biological activity of calcifying organisms and exchange at the sediment-water interface (Middelburg et al., 2020) — an undergoing development in our modeling system.

In our model, the global-ocean net CO_2 outgassing driven by riverine exports reflects the stronger effect of riverine carbon on the solubility pump (CO_2 source) compared to the change in the CO_2 uptake associated with the increase in NPP. This imbalance can result from an overestimation of CO_2 outgassing driven by riverine carbon, and especially t_{DOC}. First, assuming that total loads of carbon or nutrients over each watershed are routed to the ocean is a misrepresentation, as losses and gains occur through the LOAC (W.-J. Cai, 2011). Second, t_{DOC} is degraded in coastal waters at different rates depending on its origin and subsequent labile fraction (Lønborg et al., 2020). In the present study, in addition to not accounting for refractory and labile fractions of t_{DOC}, marine and terrestrial DOC are both being remineralized at the same rate (3 months). Overall, this could lead to an overestimation of t_{DOC} remineralization and thus ocean CO_2 outgassing due to the subsequent excess of DIC. For instance, the Amazon River — the main source of riverine t_{DOC} into the ocean — contributes to almost 50% (+0.014 Pg C yr^{-1}) of the global-ocean CO_2 outgassing in response to riverine exports in our study. However, t_{DOC} from the Amazon River shows stronger stability in the coastal ocean and is exported from the continental margin to the open ocean (Medeiros et al., 2015; Louchard et al., 2021). Increasing the refractory pool of Amazon t_{DOC} could therefore decrease CO_2 outgassing in our simulations. While recent modeling studies include separate pools of refractory and labile t_{DOC} with different remineralization rates at regional scales (Louchard et al., 2021; Gibson et al., 2022; Bertin et al., 2023), the nature of t_{DOC} needs to be better accounted for in global-ocean biogeochemistry models.

5 Perspectives

Biogeochemical inputs from rivers into the ocean are subject to variability from climate change and/or human activities. Over the last century, loads of riverine exports such as nitrogen and phosphorus increased dramatically — mostly due to anthropogenic perturbations (+349% and +233%, respectively) (Lacroix et al., 2021). In the coastal ocean, this has strongly increased NPP associated with the regions in which our model depicts the strongest impact of riverine nutrients on NPP (TROP-ATL and SE-ASIA) (Lacroix et al., 2021). Over the past 20 years, fertilizers and aquaculture have been identified as global drivers of phytoplankton blooms in coastal waters (Dai et al., 2023). The load of riverine t_{DOC} also increased globally over the period 1860–2010 (+17%), due to CO_2 fertilization of terrestrial vegetation and climate change (Nakhavali et al., 2024). In the near future (2050), the global contribution of natural sources of nitrogen and phosphorus in riverine inputs is expected to continue to decrease due to land-use change, while anthropogenic sources from human waste, agriculture, and aquaculture are projected to increase for every potential Shared Socioeconomic Pathways (SSP) scenario (Beusen et al., 2022). However, the export of nutrients from anthropogenic sources to the ocean will decrease in industrialized regions such as North America, Europe (including the Russian Federation), Japan, and Oceania in most SSPs (Beusen & Bouwman, 2022). For instance, in the contiguous United States, the riverine load of nitrogen from human waste and atmospheric pollution decreased over 1930–2017 (Byrnes et al., 2020). Nonetheless, the load of nitrogen from agricultural sources kept increasing over the same period (Byrnes et al., 2020). Consequently, only the long-term adoption of the Paris Agreement and sustainable development scenarios, such as SSP1 where the use of resources and the dependency on fossil fuels are significantly reduced, would lead to better stream water quality (Beusen & Bouwman, 2022; Beusen et al., 2022). Over the 21^{st} century, the increase of ocean NPP and the associated carbon sink driven by the historical increase of nutrients loads is ex-

pected to be dampened by the increase of CO_2 outgassing from elevated terrestrial organic matter loads (S. Gao et al., 2023).

Depicting the role of riverine exports in the ocean carbon cycle remains limited by the spatial and temporal coverage/resolution of models, forcing products, and observations. As river discharge is associated with suspended particulate loads, ocean color retrievals from spaceborne instruments can be an effective tool for monitoring river plumes systems. However, the complexity of optical properties and their large space-time variability requires high-resolution sensors to capture the actual constituents of ocean biogeochemistry. The recently launched Plankton, Aerosol, Cloud, ocean Ecosystem (PACE) satellite mission (https://pace.oceansciences.org/) and its onboard high-resolution spectrometer will bring new insights into the water quality of coastal regions near river mouths. Combined, with river discharge retrievals from the Surface Water and Ocean Topography (SWOT, https://swot.jpl.nasa.gov/), combined spaceborne observations of ocean color and terrestrial fluxes of freshwater into the ocean will pave the way for an integrated Earth Observation System, where the connection between the land and the ocean will be better understood. While effective, these satellite missions are expensive and should not replace critical in-situ and ground-truthed observations. We highlight that ambitious spaceborne missions can indeed be complemented by more modest initiatives, such as citizen science or stakeholder engagement to monitor water quality in river systems (Abbott et al., 2018).

6 Conclusion

Our simulations suggest that the role of present-day riverine exports is moderate, with an outgassing of 0.03 Pg C yr^{-1} to the atmosphere, globally. We find that riverine inputs drive contrasting regional patterns in air-sea CO_2 flux. Terrestrial dissolved carbon, and especially t_{DOC}, contributes to an outgassing of CO_2 through a reduction of the ocean's solubility pump. Terrestrial nutrients, and in particular t_{DIN}, fertilizes phytoplankton and increases marine NPP and the associated carbon biomass. Thus, terrestrial nutrients such as inorganic nitrogen and silica enhance the uptake of atmospheric CO_2 into the ocean. While outgassing of CO_2 is primarily located near river mouths, the fertilization by riverine nitrogen and silica spreads further offshore and into the open ocean. In carbon-dominated margins such as ARCT or TROP-ATL, rivers contribute a large source of CO_2 from the ocean to the atmosphere. However, in nitrogen-dominated margins such as SE-ASIA, rivers drive a large sink of atmospheric CO_2 into the ocean. This work highlights that a better quantification of lateral riverine exports and the incorporation of these fluxes in global models is pivotal for regional and global carbon budgets. Conducting sensitivity experiments could support national policy decisions and inform climate resilience strategies for land and marine practices.

Acknowledgments

A portion of this research was carried out at the Jet Propulsion Laboratory, California Institute of Technology, under a contract with the National Aeronautics and Space Administration (80NM0018D0004). Support from the Carbon Cycle Science (CCS) and Carbon Monitoring Systems (CMS) programs are acknowledged. High-end computing resources were provided by the NASA Advanced Supercomputing (NAS) Division of the Ames Research Center. Government sponsorship acknowledged.

Open Research

ECCO-Darwin model output is available at the ECCO Data Portal: http://data.nas.nasa.gov/ecco/. Model code and platform-independent instructions for running the ECCO-Darwin sim-

ulations used in this paper and generating runoff forcing are available at: 10.5281/zenodo.10562713.

References

Abbott, B. W., Moatar, F., Gauthier, O., Fovet, O., Antoine, V., & Ragueneau, O. (2018). Trends and seasonality of river nutrients in agricultural catchments: 18years of weekly citizen science in france. *Science of The Total Environment*, *624*, 845-858. Retrieved from `https://www.sciencedirect.com/science/article/pii/S0048969717336033` doi: https://doi.org/10.1016/j.scitotenv.2017.12.176

Amiotte Suchet, P., Probst, J.-L., & Ludwig, W. (2003). Worldwide distribution of continental rock lithology: Implications for the atmospheric/soil co2 uptake by continental weathering and alkalinity river transport to the oceans. *Global Biogeochemical Cycles*, *17*(2).

Andrews, A., Kofler, J., Trudeau, M., Williams, J., Neff, D., Masarie, K., ... others (2014). Co 2, co, and ch 4 measurements from tall towers in the noaa earth system research laboratory's global greenhouse gas reference network: Instrumentation, uncertainty analysis, and recommendations for future high-accuracy greenhouse gas monitoring efforts. *Atmospheric Measurement Techniques*, *7*(2), 647–687.

Araujo, M., Noriega, C., & Lefèvre, N. (2014). Nutrients and carbon fluxes in the estuaries of major rivers flowing into the tropical atlantic. *Frontiers in Marine Science*, *1*. Retrieved from `https://www.frontiersin.org/articles/10.3389/fmars.2014.00010` doi: 10.3389/fmars.2014.00010

Battin, T. J., Lauerwald, R., Bernhardt, E. S., Bertuzzo, E., Gener, L. G., Hall Jr, R. O., ... others (2023). River ecosystem metabolism and carbon biogeochemistry in a changing world. *Nature*, *613*(7944), 449–459.

Bertin, C., Carroll, D., Menemenlis, D., Dutkiewicz, S., Zhang, H., Matsuoka, A., ... others (2023). Biogeochemical river runoff drives intense coastal arctic ocean co2 outgassing. *Geophysical Research Letters*, *50*(8), e2022GL102377.

Beusen, A. H. W., & Bouwman, A. F. (2022). Future projections of river nutrient export to the global coastal ocean show persisting nitrogen and phosphorus distortion. *Frontiers in Water*, *4*, 893585.

Beusen, A. H. W., Doelman, J. C., Van Beek, L. P. H., Van Puijenbroek, P. J. T. M., Mogollón, J. M., Van Grinsven, H. J. M., ... Bouwman, A. F. (2022). Exploring river nitrogen and phosphorus loading and export to global coastal waters in the shared socio-economic pathways. *Global Environmental Change*, *72*, 102426.

Bloom, A. A., Bowman, K. W., Liu, J., Konings, A. G., Worden, J. R., Parazoo, N. C., ... others (2020). Lagged effects regulate the inter-annual variability of the tropical carbon balance. *Biogeosciences*, *17*(24), 6393–6422.

Brix, H., Menemenlis, D., Hill, C., Dutkiewicz, S., Jahn, O., Wang, D., ... Zhang, H. (2015). Using green's functions to initialize and adjust a global, eddying ocean biogeochemistry general circulation model. *Ocean Modelling*, *95*, 1–14.

Byrnes, D. K., Van Meter, K. J., & Basu, N. B. (2020). Long-term shifts in u.s. nitrogen sources and sinks revealed by the new trend-nitrogen data set (1930–2017). *Global Biogeochemical Cycles*, *34*(9), e2020GB006626. Retrieved from `https://agupubs.onlinelibrary.wiley.com/doi/abs/10.1029/2020GB006626` (e2020GB006626 2020GB006626) doi: https://doi.org/10.1029/2020GB006626

Cai, W., Chen, C. A., & Borges, A. (2013). Carbon dioxide dynamics and fluxes in coastal waters influenced by river plumes. *Biogeochemical Dynamics at Major River-Coastal Interfaces, edited by: Bianchi, TS, Allison MA, and Cai, W.-J., Cambridge University Press, Cambridge*, 155–173.

Cai, W.-J. (2011). Estuarine and coastal ocean carbon paradox: Co2 sinks or sites of terrestrial carbon incineration? *Annual review of marine science*, *3*, 123–145.

Cai, W.-J., Hu, X., Huang, W.-J., Jiang, L.-Q., Wang, Y., Peng, T.-H., & Zhang, X. (2010). Alkalinity distribution in the western north atlantic ocean margins. *Journal of Geophysical Research: Oceans*, *115*(C8). Retrieved from https://agupubs.onlinelibrary.wiley.com/doi/abs/10.1029/2009JC005482 doi: https://doi.org/10.1029/2009JC005482

Calmels, D., Gaillardet, J., Brenot, A., & France-Lanord, C. (2007). Sustained sulfide oxidation by physical erosion processes in the mackenzie river basin: Climatic perspectives. *Geology*, *35*(11), 1003–1006.

Carroll, D., Menemenlis, D., Adkins, J., Bowman, K., Brix, H., Dutkiewicz, S., ... others (2020). The ecco-darwin data-assimilative global ocean biogeochemistry model: Estimates of seasonal to multidecadal surface ocean pco2 and air-sea co2 flux. *Journal of Advances in Modeling Earth Systems*, *12*(10), e2019MS001888.

Carroll, D., Menemenlis, D., Dutkiewicz, S., Lauderdale, J. M., Adkins, J. F., Bowman, K. W., ... others (2022). Attribution of space-time variability in global-ocean dissolved inorganic carbon. *Global biogeochemical cycles*, *36*(3), e2021GB007162.

Carroll, D., Menemenlis, D., Zhang, H., Mazloff, M., McKinley, G., Fay, A., ... Fenty, I. (2024, February). *Evaluation of the ECCO-DarwinOcean Biogeochemistry State Estimatevs. In-situ Observations.* Zenodo. Retrieved from https://doi.org/10.5281/zenodo.10627664 doi: 10.5281/zenodo.10627664

Carvalho, K., & Wang, S. (2020). Sea surface temperature variability in the arctic ocean and its marginal seas in a changing climate: Patterns and mechanisms. *Global and Planetary Change*, *193*, 103265. Retrieved from https://www.sciencedirect.com/science/article/pii/S0921818120301569 doi: https://doi.org/10.1016/j.gloplacha.2020.103265

Cheng, G., & Wu, T. (2007). Responses of permafrost to climate change and their environmental significance, qinghai-tibet plateau. *Journal of Geophysical Research: Earth Surface*, *112*(F2).

Cleveland, C. C., Wieder, W. R., Reed, S. C., & Townsend, A. R. (2010). Experimental drought in a tropical rain forest increases soil carbon dioxide losses to the atmosphere. *Ecology*, *91*(8), 2313–2323.

Cotrim da Cunha, L., Buitenhuis, E. T., Le Quéré, C., Giraud, X., & Ludwig, W. (2007). Potential impact of changes in river nutrient supply on global ocean biogeochemistry. *Global Biogeochemical Cycles*, *21*(4).

da Cunha, L. C., & Buitenhuis, E. (2013). Riverine influence on the tropical atlantic ocean biogeochemistry. *Biogeosciences*, *10*(10), 6357–6373.

Dai, Y., Yang, S., Zhao, D., Hu, C., Xu, W., Anderson, D. M., ... others (2023). Coastal phytoplankton blooms expand and intensify in the 21st century. *Nature*, *615*(7951), 280–284.

De Verneil, A., Lachkar, Z., Smith, S., & Lévy, M. (2021). Evaluating the arabian sea as a regional source of atmospheric co 2: seasonal variability and drivers. *Biogeosciences Discussions*, *2021*, 1–38.

Drake, T. W., Raymond, P. A., & Spencer, R. G. (2018). Terrestrial carbon inputs to inland waters: A current synthesis of estimates and uncertainty. *Limnology and Oceanography Letters*, *3*(3), 132–142.

Dubois, K. D., Lee, D., & Veizer, J. (2010). Isotopic constraints on alkalinity, dissolved organic carbon, and atmospheric carbon dioxide fluxes in the mississippi river. *Journal of Geophysical Research: Biogeosciences*, *115*(G2). Retrieved from https://agupubs.onlinelibrary.wiley.com/doi/abs/10.1029/2009JG001102 doi: https://doi.org/10.1029/2009JG001102

Duhamel, S., Diaz, J. M., Adams, J. C., Djaoudi, K., Steck, V., & Waggoner, E. M. (2021). Phosphorus as an integral component of global marine biogeochemistry.

Nature Geoscience, *14*(6), 359–368.

Fekete, B. M., Vörösmarty, C. J., & Grabs, W. (2002). High-resolution fields of global runoff combining observed river discharge and simulated water balances. *Global Biogeochemical Cycles*, *16*(3), 15–1–15–10.

Feng, Y., Menemenlis, D., Xue, H., Zhang, H., Carroll, D., Du, Y., & Wu, H. (2021). Improved representation of river runoff in estimating the circulation and climate of the ocean version 4 (eccov4) simulations: implementation, evaluation, and impacts to coastal plume regions. *Geoscientific Model Development*, *14*(3), 1801–1819.

Fennel, K., & Testa, J. M. (2019). Biogeochemical controls on coastal hypoxia. *Annual review of marine science*, *11*, 105–130.

Fleischer, K., Rammig, A., De Kauwe, M. G., Walker, A. P., Domingues, T. F., Fuchslueger, L., ... others (2019). Amazon forest response to co2 fertilization dependent on plant phosphorus acquisition. *Nature Geoscience*, *12*(9), 736–741.

Follows, M. J., Ito, T., & Dutkiewicz, S. (2006). On the solution of the carbonate chemistry system in ocean biogeochemistry models. *Ocean Modelling*, *12*(3-4), 290–301.

Forget, G., Campin, J.-M., Heimbach, P., Hill, C., Ponte, R., & Wunsch, C. (2015). Ecco version 4: An integrated framework for non-linear inverse modeling and global ocean state estimation. *Geoscientific Model Development*, *8*(10), 3071–3104.

Friedlingstein, P., O'sullivan, M., Jones, M. W., Andrew, R. M., Bakker, D. C., Hauck, J., ... others (2023). Global carbon budget 2023. *Earth System Science Data*, *15*(12), 5301–5369.

Frings, P. J., Clymans, W., Fontorbe, G., Christina, L., & Conley, D. J. (2016). The continental si cycle and its impact on the ocean si isotope budget. *Chemical Geology*, *425*, 12–36.

Gao, S., Schwinger, J., Tjiputra, J., Bethke, I., Hartmann, J., Mayorga, E., & Heinze, C. (2023). Riverine impact on future projections of marine primary production and carbon uptake. *Biogeosciences*, *20*(1), 93–119.

Gao, Y., Yang, T., Wang, Y., & Yu, G. (2017). Fate of river-transported carbon in china: implications for carbon cycling in coastal ecosystems. *Ecosystem Health and Sustainability*, *3*(3), e01265. Retrieved from `https://spj.science.org/doi/abs/10.1002/ehs2.1265` doi: 10.1002/ehs2.1265

Gaspar, P., Grégoris, Y., & Lefevre, J.-M. (1990). A simple eddy kinetic energy model for simulations of the oceanic vertical mixing: Tests at station papa and long-term upper ocean study site. *Journal of Geophysical Research: Oceans*, *95*(C9), 16179–16193.

Ghosh, J., Chakraborty, K., Chanda, A., Akhand, A., Bhattacharya, T., Das, S., ... Wells, M. (2021). Outwelling of total alkalinity and dissolved inorganic carbon from the hooghly river to the adjacent coastal bay of bengal. *Environmental Monitoring and Assessment*, *193*(7), 415.

Gibson, G. A., Elliot, S., Clement Kinney, J., Piliouras, A., & Jeffery, N. (2022). Assessing the potential impact of river chemistry on arctic coastal production. *Frontiers in Marine Science*, *9*, 738363. Retrieved from `https://www.frontiersin.org/articles/10.3389/fmars.2022.738363` doi: 10.3389/fmars.2022.738363

Gomez, F. A., Lee, S.-K., Stock, C. A., Ross, A. C., Resplandy, L., Siedlecki, S. A., ... Salisbury, J. E. (2023). Rc4uscoast: a river chemistry dataset for regional ocean model applications in the us east coast, gulf of mexico, and us west coast. *Earth System Science Data*, *15*(5), 2223–2234.

Guo, J., Wang, F., Vogt, R. D., Zhang, Y., & Liu, C.-Q. (2015). Anthropogenically enhanced chemical weathering and carbon evasion in the yangtze basin. *Scientific reports*, *5*(1), 11941.

Hagemann, S., & Dümenil, L. (1997). A parametrization of the lateral waterflow for

the global scale. *Climate dynamics*, *14*, 17–31.

Hagemann, S., & Gates, L. D. (2003). Improving a subgrid runoff parameterization scheme for climate models by the use of high resolution data derived from satellite observations. *Climate Dynamics*, *21*, 349–359.

Hartmann, J., Jansen, N., Dürr, H. H., Kempe, S., & Köhler, P. (2009). Global co2-consumption by chemical weathering: What is the contribution of highly active weathering regions? *Global and Planetary Change*, *69*(4), 185–194.

Hartmann, J., Lauerwald, R., & Moosdorf, N. (2014). A brief overview of the global river chemistry database, glorich. *Procedia Earth and Planetary Science*, *10*, 23–27.

Holmes, R. M., McClelland, J. W., Peterson, B. J., Tank, S. E., Bulygina, E., Eglinton, T. I., ... others (2012). Seasonal and annual fluxes of nutrients and organic matter from large rivers to the arctic ocean and surrounding seas. *Estuaries and Coasts*, *35*, 369–382.

Hood, R. R., Rixen, T., Levy, M., Hansell, D. A., Coles, V. J., & Lachkar, Z. (2023). *Oxygen, carbon and ph variability in the indian ocean.* Elsevier.

Ianson, D., Feely, R. A., Sabine, C. L., & Juranek, L. W. (2009). Features of coastal upwelling regions that determine net air-sea co 2 flux. *Journal of oceanography*, *65*, 677–687.

Jersild, A., Landschützer, P., Gruber, N., & Bakker, D. (2023). *An observation-based global monthly gridded sea surface pco2 and air-sea co2 flux product from 1982 onward and its monthly climatology* (Vol. 160558).

Jones, M. W., Coppola, A. I., Santín, C., Dittmar, T., Jaffé, R., Doerr, S. H., & Quine, T. A. (2020). Fires prime terrestrial organic carbon for riverine export to the global oceans. *Nature communications*, *11*(1), 2791.

Jouanno, J., Moquet, J.-S., Berline, L., Radenac, M.-H., Santini, W., Changeux, T., ... others (2021). Evolution of the riverine nutrient export to the tropical atlantic over the last 15 years: is there a link with sargassum proliferation? *Environmental Research Letters*, *16*(3), 034042.

Kartadikaria, A. R., Watanabe, A., Nadaoka, K., Adi, N. S., Prayitno, H. B., Soemorumekso, S., ... others (2015). Co2 sink/source characteristics in the tropical indonesian seas. *Journal of Geophysical Research: Oceans*, *120*(12), 7842–7856.

Krachler, R., Jirsa, F., & Ayromlou, S. (2005). Factors influencing the dissolved iron input by river water to the open ocean. *Biogeosciences*, *2*(4), 311–315.

Krinner, G., Viovy, N., de Noblet-Ducoudré, N., Ogée, J., Polcher, J., Friedlingstein, P., ... Prentice, I. C. (2005). A dynamic global vegetation model for studies of the coupled atmosphere-biosphere system. *Global Biogeochemical Cycles*, *19*(1).

Lacroix, F., Ilyina, T., & Hartmann, J. (2020). Oceanic co 2 outgassing and biological production hotspots induced by pre-industrial river loads of nutrients and carbon in a global modeling approach. *Biogeosciences*, *17*(1), 55–88.

Lacroix, F., Ilyina, T., Mathis, M., Laruelle, G. G., & Regnier, P. (2021). Historical increases in land-derived nutrient inputs may alleviate effects of a changing physical climate on the oceanic carbon cycle. *Global change biology*, *27*(21), 5491–5513.

Landschützer, P., Gruber, N., & Bakker, D. C. (2016). Decadal variations and trends of the global ocean carbon sink. *Global Biogeochemical Cycles*, *30*(10), 1396–1417.

Laruelle, G. G., Goossens, N., Arndt, S., Cai, W.-J., & Regnier, P. (2017). Air–water co 2 evasion from us east coast estuaries. *Biogeosciences*, *14*(9), 2441–2468.

Lauerwald, R., Regnier, P., Guenet, B., Friedlingstein, P., & Ciais, P. (2020). How simulations of the land carbon sink are biased by ignoring fluvial carbon transfers: A case study for the amazon basin. *One Earth*, *3*(2), 226-236. Retrieved from `https://www.sciencedirect.com/science/article/pii/S2590332220303535` doi: https://doi.org/10.1016/j.oneear.2020.07.009

Laurent, A., Fennel, K., Cai, W.-J., Huang, W.-J., Barbero, L., & Wanninkhof, R. (2017). Eutrophication-induced acidification of coastal waters in the northern gulf of mexico: Insights into origin and processes from a coupled physical-biogeochemical model. *Geophysical Research Letters*, *44*(2), 946–956.

Lee, R. Y., Seitzinger, S., & Mayorga, E. (2016). Land-based nutrient loading to lmes: a global watershed perspective on magnitudes and sources. *Environmental development*, *17*, 220–229.

Le Fouest, V., Babin, M., & Tremblay, J.-É. (2013). The fate of riverine nutrients on arctic shelves. *Biogeosciences*, *10*(6), 3661–3677.

Le Fouest, V., Manizza, M., Tremblay, B., & Babin, M. (2015). Modelling the impact of riverine don removal by marine bacterioplankton on primary production in the arctic ocean. *Biogeosciences*, *12*(11), 3385–3402. Retrieved from `https://bg.copernicus.org/articles/12/3385/2015/` doi: 10.5194/bg-12-3385-2015

Li, H.-M., Tang, H.-J., Shi, X.-Y., Zhang, C.-S., & Wang, X.-L. (2014). Increased nutrient loads from the changjiang (yangtze) river have led to increased harmful algal blooms. *Harmful Algae*, *39*, 92–101.

Li, M., Peng, C., Wang, M., Xue, W., Zhang, K., Wang, K., ... Zhu, Q. (2017). The carbon flux of global rivers: A re-evaluation of amount and spatial patterns. *Ecological Indicators*, *80*, 40–51.

Li, M., Peng, C., Zhou, X., Yang, Y., Guo, Y., Shi, G., & Zhu, Q. (2019). Modeling global riverine doc flux dynamics from 1951 to 2015. *Journal of Advances in Modeling Earth Systems*, *11*(2), 514-530. Retrieved from `https://agupubs.onlinelibrary.wiley.com/doi/abs/10.1029/2018MS001363` doi: https://doi.org/10.1029/2018MS001363

Lønborg, C., Carreira, C., Jickells, T., & Álvarez-Salgado, X. A. (2020, jun). Impacts of Global Change on Ocean Dissolved Organic Carbon (DOC) Cycling. *Frontiers in Marine Science*, *7*. doi: 10.3389/fmars.2020.00466

Louchard, D., Gruber, N., & Münnich, M. (2021). The impact of the amazon on the biological pump and the air-sea co2 balance of the western tropical atlantic. *Global Biogeochemical Cycles*, *35*(6), e2020GB006818.

Maavara, T., Lauerwald, R., Regnier, P., & Van Cappellen, P. (2017). Global perturbation of organic carbon cycling by river damming. *Nature communications*, *8*(1), 15347.

Mahowald, N. M., Engelstaedter, S., Luo, C., Sealy, A., Artaxo, P., Benitez-Nelson, C., ... others (2009). Atmospheric iron deposition: global distribution, variability, and human perturbations. *Annual review of marine science*, *1*, 245–278.

Manizza, M., Follows, M. J., Dutkiewicz, S., Menemenlis, D., McClelland, J. W., Hill, C. N., ... Key, R. M. (2011). A model of the arctic ocean carbon cycle. *Journal of Geophysical Research: Oceans*, *116*(C12). Retrieved from `https://agupubs.onlinelibrary.wiley.com/doi/abs/10.1029/2011JC006998` doi: https://doi.org/10.1029/2011JC006998

Manizza, M., Menemenlis, D., Zhang, H., & Miller, C. E. (2019). Modeling the recent changes in the arctic ocean co2 sink (2006–2013). *Global Biogeochemical Cycles*, *33*(3), 420–438.

Mathis, M., Lacroix, F., Hagemann, S., Nielsen, D. M., Ilyina, T., & Schrum, C. (2024). Enhanced co2 uptake of the coastal ocean is dominated by biological carbon fixation. *Nature Climate Change*, 1–7.

Mathis, M., Logemann, K., Maerz, J., Lacroix, F., Hagemann, S., Chegini, F., ... Schrum, C. (2022). Seamless integration of the coastal ocean in global marine carbon cycle modeling. *Journal of Advances in Modeling Earth Systems*, *14*(8), e2021MS002789.

Mayorga, E., Seitzinger, S. P., Harrison, J. A., Dumont, E., Beusen, A. H., Bouwman, A., ... Van Drecht, G. (2010). Global nutrient export from watersheds 2

(news 2): model development and implementation. *Environmental Modelling & Software*, *25*(7), 837–853.

Medeiros, P. M., Seidel, M., Ward, N. D., Carpenter, E. J., Gomes, H. R., Niggemann, J., ... Dittmar, T. (2015). Fate of the amazon river dissolved organic matter in the tropical atlantic ocean. *Global Biogeochemical Cycles*, *29*(5), 677–690.

Menemenlis, D., Fukumori, I., & Lee, T. (2005). Using green's functions to calibrate an ocean general circulation model. *Monthly weather review*, *133*(5), 1224–1240.

Meybeck, M., & Vörösmarty, C. (1999). Global transfer of carbon by rivers. *Global Change Newsletter*, *37*, 18–19.

Michael Beman, J., Arrigo, K. R., & Matson, P. A. (2005). Agricultural runoff fuels large phytoplankton blooms in vulnerable areas of the ocean. *Nature*, *434*(7030), 211–214.

Middelburg, J. J., Soetaert, K., & Hagens, M. (2020). Ocean alkalinity, buffering and biogeochemical processes. *Reviews of Geophysics*, *58*(3), e2019RG000681. Retrieved from `https://agupubs.onlinelibrary.wiley.com/doi/abs/10.1029/2019RG000681` (e2019RG000681 2019RG000681) doi: https://doi.org/10.1029/2019RG000681

Mol, J., Thomas, H., Myers, P. G., Hu, X., & Mucci, A. (2018). Inorganic carbon fluxes on the mackenzie shelf of the beaufort sea. *Biogeosciences*, *15*(4), 1011–1027.

Monteith, D. T., Stoddard, J. L., Evans, C. D., De Wit, H. A., Forsius, M., Høgåsen, T., ... others (2007). Dissolved organic carbon trends resulting from changes in atmospheric deposition chemistry. *Nature*, *450*(7169), 537–540.

Mortenson, E., Steiner, N., Monahan, A. H., Hayashida, H., Sou, T., & Shao, A. (2020). Modeled impacts of sea ice exchange processes on arctic ocean carbon uptake and acidification (1980–2015). *Journal of Geophysical Research: Oceans*, *125*(7), e2019JC015782. Retrieved from `https://agupubs.onlinelibrary.wiley.com/doi/abs/10.1029/2019JC015782` (e2019JC015782 10.1029/2019JC015782) doi: https://doi.org/10.1029/2019JC015782

Nakhavali, M. A., Lauerwald, R., Regnier, P., & Friedlingstein, P. (2024). Historical trends and drivers of the laterally transported terrestrial dissolved organic carbon to river systems. *Science of The Total Environment*, *917*, 170560. Retrieved from `https://www.sciencedirect.com/science/article/pii/S0048969724006971` doi: https://doi.org/10.1016/j.scitotenv.2024.170560

Nishina, K., Ito, A., Zhou, F., Yan, X., Hayashi, S., & Winiwarter, W. (2021, aug). Historical trends of riverine nitrogen loading from land to the east china sea: a model-based evaluation. *Environmental Research Communications*, *3*(8), 085005. Retrieved from `https://dx.doi.org/10.1088/2515-7620/ac1ce8` doi: 10.1088/2515-7620/ac1ce8

Patra, P. K., Canadell, J. G., Houghton, R. A., Piao, S. L., Oh, N.-H., Ciais, P., ... Lasco, R. (2013). The carbon budget of south asia. *Biogeosciences*, *10*(1), 513–527. Retrieved from `https://bg.copernicus.org/articles/10/513/2013/` doi: 10.5194/bg-10-513-2013

Piao, S. L., Ito, A., Li, S. G., Huang, Y., Ciais, P., Wang, X. H., ... Zhu, B. (2012). The carbon budget of terrestrial ecosystems in east asia over the last two decades. *Biogeosciences*, *9*(9), 3571–3586. Retrieved from `https://bg.copernicus.org/articles/9/3571/2012/` doi: 10.5194/bg-9-3571-2012

Probst, J.-L., Mortatti, J., & Tardy, Y. (1994). Carbon river fluxes and weathering co2 consumption in the congo and amazon river basins. *Applied Geochemistry*, *9*(1), 1–13.

Raymond, P. A., Oh, N.-H., Turner, R. E., & Broussard, W. (2008). Anthropogenically enhanced fluxes of water and carbon from the mississippi river. *Nature*, *451*(7177), 449–452.

Regnier, P., Friedlingstein, P., Ciais, P., Mackenzie, F. T., Gruber, N., Janssens, I. A., ... others (2013). Anthropogenic perturbation of the carbon fluxes from land to ocean. *Nature geoscience*, *6*(8), 597–607.

Regnier, P., Resplandy, L., Najjar, R. G., & Ciais, P. (2022). The land-to-ocean loops of the global carbon cycle. *Nature*, *603*(7901), 401–410.

Resplandy, L., Keeling, R., Rödenbeck, C., Stephens, B., Khatiwala, S., Rodgers, K., ... Tans, P. (2018). Revision of global carbon fluxes based on a reassessment of oceanic and riverine carbon transport. *Nature Geoscience*, *11*(7), 504–509.

Riquetti, N. B., Beskow, S., Guo, L., & Mello, C. R. (2023). Soil erosion assessment in the amazon basin in the last 60 years of deforestation. *Environmental Research*, *236*, 116846. Retrieved from `https://www.sciencedirect.com/science/article/pii/S001393512301650X` doi: https://doi.org/10.1016/j.envres.2023.116846

Robertson, G. P., & Rosswall, T. (1986). Nitrogen in west africa: the regional cycle. *Ecological Monographs*, *56*(1), 43–72.

Rödenbeck, C. (2005). Estimating CO2 sources and sinks from atmospheric mixing ratio measurements using a global inversion of atmospheric transport. *Technical reports*.

Rödenbeck, C., Keeling, R. F., Bakker, D. C. E., Metzl, N., Olsen, A., Sabine, C., & Heimann, M. (2013). Global surface-ocean pCO_2 and sea-air CO_2 flux variability from an observation-driven ocean mixed-layer scheme. *Ocean Science*, *9*(2), 193–216.

Samanta, S., Dalai, T. K., Pattanaik, J. K., Rai, S. K., & Mazumdar, A. (2015). Dissolved inorganic carbon (DIC) and its $\delta^{13}C$ in the Ganga (Hooghly) River estuary, India: Evidence of DIC generation via organic carbon degradation and carbonate dissolution. *Geochimica et Cosmochimica Acta*, *165*, 226-248. Retrieved from `https://www.sciencedirect.com/science/article/pii/S0016703715003658` doi: https://doi.org/10.1016/j.gca.2015.05.040

Savenko, V. S., & Savenko, A. V. (2021). The main features of phosphorus transport in world rivers. *Water*, *14*(1), 16.

Seitzinger, S. P., Mayorga, E., Bouwman, A. F., Kroeze, C., Beusen, A. H., Billen, G., ... others (2010). Global river nutrient export: A scenario analysis of past and future trends. *Global biogeochemical cycles*, *24*(4).

Sharples, J., Middelburg, J. J., Fennel, K., & Jickells, T. D. (2017). What proportion of riverine nutrients reaches the open ocean? *Global Biogeochemical Cycles*, *31*(1), 39–58.

Singh, A., & Ramesh, R. (2011). Contribution of riverine dissolved inorganic nitrogen flux to new production in the coastal northern indian ocean: an assessment. *International Journal of Oceanography*, *2011*.

Smith, S. V., Swaney, D. P., Talaue-Mcmanus, L., Bartley, J. D., Sandhei, P. T., McLAUGHLIN, C. J., ... others (2003). Humans, hydrology, and the distribution of inorganic nutrient loading to the ocean. *Bioscience*, *53*(3), 235–245.

Song, C., Wang, G., Mao, T., Huang, K., Sun, X., Hu, Z., ... Raymond, P. A. (2020). Spatiotemporal variability and sources of dic in permafrost catchments of the yangtze river source region: Insights from stable carbon isotope and water chemistry. *Water Resources Research*, *56*(1), e2019WR025343. Retrieved from `https://agupubs.onlinelibrary.wiley.com/doi/abs/10.1029/2019WR025343` (e2019WR025343 2019WR025343) doi: https://doi.org/10.1029/2019WR025343

Spencer, R. G. M., Mann, P. J., Dittmar, T., Eglinton, T. I., McIntyre, C., Holmes, R. M., ... Stubbins, A. (2015). Detecting the signature of permafrost thaw in arctic rivers. *Geophysical Research Letters*, *42*(8), 2830-2835. Retrieved from `https://agupubs.onlinelibrary.wiley.com/doi/abs/10.1002/2015GL063498` doi: https://doi.org/10.1002/2015GL063498

Suchet, P. A., & Probst, J.-L. (1995). A global model for present-day atmo-

spheric/soil co2 consumption by chemical erosion of continental rocks (gem-co2). *Tellus B*, *47*(1-2), 273–280.

Suzuki, T., Yamazaki, D., Tsujino, H., Komuro, Y., Nakano, H., & Urakawa, S. (2018). A dataset of continental river discharge based on jra-55 for use in a global ocean circulation model. *Journal of oceanography*, *74*, 421–429.

Tagliabue, A., Bowie, A. R., Boyd, P. W., Buck, K. N., Johnson, K. S., & Saito, M. A. (2017). The integral role of iron in ocean biogeochemistry. *Nature*, *543*(7643), 51–59.

Tank, S. E., Raymond, P. A., Striegl, R. G., McClelland, J. W., Holmes, R. M., Fiske, G. J., & Peterson, B. J. (2012). A land-to-ocean perspective on the magnitude, source and implication of dic flux from major arctic rivers to the arctic ocean. *Global Biogeochemical Cycles*, *26*(4). Retrieved from `https://agupubs.onlinelibrary.wiley.com/doi/abs/10.1029/2011GB004192` doi: https://doi.org/10.1029/2011GB004192

Terhaar, J., Lauerwald, R., Regnier, P., Gruber, N., & Bopp, L. (2021). Around one third of current arctic ocean primary production sustained by rivers and coastal erosion. *Nature Communications*, *12*(1), 169.

Tian, H., Xu, R., Pan, S., Yao, Y., Bian, Z., Cai, W.-J., ... Yang, J. (2020). Long-term trajectory of nitrogen loading and delivery from mississippi river basin to the gulf of mexico. *Global Biogeochemical Cycles*, *34*(5), e2019GB006475. Retrieved from `https://agupubs.onlinelibrary.wiley.com/doi/abs/10.1029/2019GB006475` (e2019GB006475 2019GB006475) doi: https://doi.org/10.1029/2019GB006475

Tian, H., Yao, Y., Li, Y., Shi, H., Pan, S., Najjar, R. G., ... Leung, L. R. (2023). Increased terrestrial carbon export and co2 evasion from global inland waters since the preindustrial era. *Global Biogeochemical Cycles*, *37*(10), e2023GB007776. Retrieved from `https://agupubs.onlinelibrary.wiley.com/doi/abs/10.1029/2023GB007776` (e2023GB007776 2023GB007776) doi: https://doi.org/10.1029/2023GB007776

Tivig, M., Keller, D. P., & Oschlies, A. (2021). Riverine nitrogen supply to the global ocean and its limited impact on global marine primary production: a feedback study using an earth system model. *Biogeosciences*, *18*(19), 5327–5350. Retrieved from `https://bg.copernicus.org/articles/18/5327/2021/` doi: 10.5194/bg-18-5327-2021

Tsujino, H., Urakawa, S., Nakano, H., Small, R. J., Kim, W. M., Yeager, S. G., ... others (2018). Jra-55 based surface dataset for driving ocean–sea-ice models (jra55-do). *Ocean Modelling*, *130*, 79–139.

Vishwakarma, S., Zhang, X., & Mueller, N. D. (2022). Projecting future nitrogen inputs: are we making the right assumptions? *Environmental Research Letters*, *17*(5), 054035.

Volta, C., Laruelle, G. G., Arndt, S., & Regnier, P. (2016). Linking biogeochemistry to hydro-geometrical variability in tidal estuaries: a generic modeling approach. *Hydrology and earth system sciences*, *20*(3), 991–1030.

Vörösmarty, C., Fekete, B. M., Meybeck, M., & Lammers, R. B. (2000). Global system of rivers: Its role in organizing continental land mass and defining land-to-ocean linkages. *Global Biogeochemical Cycles*, *14*(2), 599–621.

Wang, F., Wang, Y., Zhang, J., Xu, H., & Wei, X. (2007). Human impact on the historical change of co 2 degassing flux in river changjiang. *Geochemical Transactions*, *8*, 1–10.

Wang, J., Beusen, A. H., Liu, X., Van Dingenen, R., Dentener, F., Yao, Q., ... Bouwman, A. F. (2020). Spatially explicit inventory of sources of nitrogen inputs to the yellow sea, east china sea, and south china sea for the period 1970–2010. *Earth's Future*, *8*(10), e2020EF001516.

Wanninkhof, R. (1992). Relationship between wind speed and gas exchange over the

ocean. *Journal of Geophysical Research: Oceans*, *97*(C5), 7373–7382.

Ward, N. D., Megonigal, J. P., Bond-Lamberty, B., Bailey, V. L., Butman, D., Canuel, E. A., ... others (2020). Representing the function and sensitivity of coastal interfaces in earth system models. *Nature communications*, *11*(1), 2458.

Wunsch, C., & Heimbach, P. (2013). Dynamically and kinematically consistent global ocean circulation and ice state estimates. In *International geophysics* (Vol. 103, pp. 553–579). Elsevier.

Wunsch, C., Heimbach, P., Ponte, R. M., Fukumori, I., & MEMBERS, E.-G. C. (2009). The global general circulation of the ocean estimated by the ecco-consortium. *Oceanography*, *22*(2), 88–103.

Yang, M., Nelson, F. E., Shiklomanov, N. I., Guo, D., & Wan, G. (2010). Permafrost degradation and its environmental effects on the tibetan plateau: A review of recent research. *Earth-Science Reviews*, *103*(1-2), 31–44.

Zhang, J., Lu, C., Crumpton, W., Jones, C., Tian, H., Villarini, G., ... Green, D. (2022). Heavy precipitation impacts on nitrogen loading to the gulf of mexico in the 21st century: Model projections under future climate scenarios. *Earth's future*, *10*(4), e2021EF002141.

Zhong, G., Li, X., Song, J., Qu, B., Wang, F., Wang, Y., ... Xing, J. (2022). The increasing big gap of carbon sink between the western and eastern pacific in the last three decades. *Frontiers in Marine Science*, *9*. Retrieved from `https://www.frontiersin.org/articles/10.3389/fmars.2022.1088181` doi: 10.3389/fmars.2022.1088181